

1 **Rab11A regulates the constitutive secretory pathway during *Toxoplasma gondii***
2 **invasion of host cells and parasite replication**

3 Venugopal Kannan^{1§*}, Chehade Sylia^{1*}, Werkmeister Elisabeth¹, Barois Nicolas¹,
4 Periz Javier⁴, Lafont Frank¹, Tardieux Isabelle², Khalife Jamal¹, Gordon Langsley³,
5 Meissner Markus⁴ and Marion Sabrina^{1#}.

6 *contributed equally

7 #corresponding author

8

9 ¹Centre d'Infection et d'Immunité de Lille, Université de Lille, INSERM U1019,
10 CNRS UMR 8204, Institut Pasteur de Lille, Lille, France

11 [§] present address: Wellcome Centre for Integrative Parasitology, Institute of Infection,
12 Immunity and Inflammation, University of Glasgow, Glasgow, UK.

13 ² Institute for Advanced Biosciences (IAB), Membrane Dynamics of Parasite-Host
14 Cell Interactions, CNRS UMR5309, INSERM U1209, Université Grenoble Alpes,
15 Grenoble, France

16 ³Laboratoire de Biologie Cellulaire Comparative des Apicomplexes, Faculté de
17 Médecine, Université Paris Descartes—Sorbonne Paris Cité, France. INSERM U1016,
18 CNRS UMR8104, Institut Cochin, Paris, France

19 ⁴Department of Veterinary Sciences, Experimental Parasitology, Ludwig-
20 Maximilians-Universität, Munich, Germany

21

22 **Summary**

23 *Toxoplasma gondii* possesses an armada of secreted virulent factors that enable
24 parasite invasion and survival into host cells. These factors are contained in specific
25 secretory organelles, the rhoptries, micronemes and dense granules that release their
26 content upon host cell recognition. Dense granules are secreted in a constitutive
27 manner during parasite replication and play a crucial role in modulating host
28 metabolic and immune responses. While the molecular mechanisms triggering rhoptry
29 and microneme release upon host cell adhesion have been well studied, constitutive
30 secretion remains a poorly explored aspect of *T. gondii* vesicular trafficking. Here, we
31 investigated the role of the small GTPase Rab11A, a known regulator of exocytosis in
32 eukaryotic cells. Our data revealed an essential role of Rab11A in promoting the
33 cytoskeleton driven transport of DG and the release of their content into the vacuolar
34 space. Rab11A also regulates transmembrane protein trafficking and localization

35 during parasite replication, indicating a broader role of Rab11A in cargo exocytosis at
36 the plasma membrane. Moreover, we found that Rab11A also regulates extracellular
37 parasite motility and adhesion to host cells. In line with these findings, MIC2
38 secretion was altered in Rab11A-defective parasites, which also exhibited severe
39 morphological defects. Strikingly, by live imaging we observed a polarized
40 accumulation of Rab11A-positive vesicles and dense granules at the apical pole of
41 extracellular motile parasites suggesting that a Rab11A-dependent apically polarized
42 transport of cargo regulates parasite motility.

43

44

45 **Introduction**

46 *Toxoplasma gondii* (*T. gondii*) is an obligatory intracellular parasite that belongs to
47 the phylum *Apicomplexa*, typified by the presence of specific apical secretory
48 organelles, the rhoptries and the micronemes. Upon contact with the host cell, rhoptry
49 (ROP) and microneme (MIC) proteins are released and promote parasite entry by
50 driving the formation of a tight parasite-host cell adhesive membrane structure (called
51 the circular junction) [1]. ROP proteins also contribute to building the
52 parasitophorous vacuole (PV), within which the parasite rapidly replicates. The
53 molecular mechanisms regulating MIC exocytosis have been well studied leading to
54 the discovery of specific parasite signaling pathways triggering their secretion upon
55 parasite adhesion to host cells [2] [3]. Dense granules (DG) are also parasite secretory
56 organelles essential for parasite survival, which release effectors modulating host
57 immune and metabolic responses [4]. Dense granule proteins (GRA) also promote the
58 formation of an intravacuolar nanotubular network (IVN), which interconnects
59 parasites during intracellular replication, thereby ensuring the synchronicity of the
60 successive divisions [5] [6] [7]. The IVN also connects the parasite to the PV
61 membrane (PVM), presumably enhancing parasite exchanges with its host, notably
62 for nutrient retrieval and parasite effector release into the host cytosol [8]. In contrast
63 to micronemes and rhoptries, DGs are randomly distributed in the parasite cytosol and
64 the mechanisms regulating their exocytosis at the parasite plasma membrane (PM)
65 have not been elucidated. In Metazoan, the process of exocytosis implies the active
66 transport of secretory vesicles to the PM, and the secretion of their content into the
67 extracellular environment or their insertion into the PM. In mammalian cells and
68 plants, two different exocytic routes have been described: the “constitutive secretory

69 pathway” supports the sorting of newly synthesized proteins from the endoplasmic
70 reticulum, through the Golgi apparatus to the PM, while, the “recycling pathway”
71 targets to the cell surface internalized material that has been transported to and sorted
72 in the pericentriolar or peripheral recycling endosomes [9]. In *T. gondii*, DGs are
73 considered to be the default constitutive secretory pathway based on the observation
74 that the SAG1-GFP fusion protein (full product or truncated of its GPI anchor
75 (SAG1ΔGPI)) was found to be transported by DGs before to being released into the
76 vacuolar space [10]. In addition, proteins whose specific motifs targeting them to
77 other secretory organelles have been deleted are localized in DGs [11] [12]. Yet, there
78 is so far no evidence that transmembrane proteins navigate through the DGs to reach
79 the PM of the parasite.

80 The small Rab GTPases belong to the Ras small G protein subfamily and operate as
81 molecular switches that alternate between two conformational states: the GTP-bound
82 “active” form and the GDP-bound “inactive” form [13]. Through their interactions
83 with various effectors, such as coat components, molecular motors and soluble NSF
84 attachment protein receptors (SNAREs), the Rab GTPases serve as multifaceted
85 organizers of almost all membrane trafficking processes, including vesicle budding
86 from the donor compartment, vesicle transport along cytoskeleton tracks and vesicle
87 tethering and fusion at the acceptor membrane [13] [14] [15]. Among the Rab
88 GTPases, Rab11 regulates the constitutive secretory and recycling pathways, thus
89 controlling secretion at the PM [14] [15] [16]. In mammalian cells, Rab11 regulates
90 vesicle transport via their anchoring to both, microtubule [17] and actin-based
91 molecular motors [18]. In addition, Rab11A promotes the tethering of recycling
92 vesicles to the PM in concert with the exocyst complex [19] [20] [21]. Through
93 multiple interactions with effector molecules, Rab11 influences numerous cellular
94 functions including ciliogenesis [22], cytokinesis [23] and cell migration [24] [25]. In
95 contrast to humans, which express over 70 Rabs, *T. gondii* possesses a limited number
96 of 13 Rabs that include two isoforms of Rab11, Rab11A and Rab11B [26]. In *T.*
97 *gondii* as well as in the related apicomplexan geni *Plasmodium spp.*, Rab11A-
98 defective parasites are unable to complete cytokinesis and show marked defects in the
99 exocytosis-assisted process that leads to proper individualization of daughter cells,
100 otherwise posteriorly connected [27] [28] [29]. In *Plasmodium*, this process was
101 suggested to be regulated by a PI4K-Rab11A mediated secretion of vesicles from the

102 TGN to the PM [28] [29]. Here, we further explored the functions of Rab11A in *T.*
103 *gondii* and demonstrated its key role in the regulation of DG exocytosis and
104 transmembrane protein delivery at the parasite PM. We also unraveled a novel role
105 for Rab11A in extracellular parasite adhesion and motility, thereby contributing to
106 host cell invasion.

107

108 **Results**

109

110 **Rab11A localizes to dynamic cytoplasmic vesicles**

111 To investigate *T. gondii* Rab11A localization, we raised a polyclonal antibody in
112 mice, which recognized a unique protein at the expected size of 25kDa in a total
113 extract of type I RH Δ *Ku80* parasites (Fig 1A). Next, we performed
114 immunofluorescence assays (IFA) in fixed RH Δ *Ku80* tachyzoites. Rab11A displays
115 distinct localizations depending on the cell cycle stage. During the G1 phase, Rab11A
116 is localized in cytoplasmic vesicles and as previously described [27], a signal was also
117 detected at the Golgi/Endosome-Like Compartment (ELC) area (Fig 1B). During
118 cytokinesis, at the onset of daughter cell budding, this Golgi/ELC localization of
119 Rab11A was clearly visualized in emerging daughter cells, together with a strong
120 enrichment of the protein at the apical tip of the growing buds, reflecting a possible
121 Rab11A-dependent transport of newly synthesized material between these two
122 locations. Rab11A also accumulates at the basal pole of the parasite both during the
123 G1 phase and cytokinesis (Fig 1B). In order to get further insights into the dynamic
124 localization of Rab11A, we used the previously established transgenic ddFKBP-myc-
125 mCherryRab11A-RH Δ *Ku80* parasites (from here designated as mcherryRab11A-WT
126 parasites) [27] [30]. In this strain, the expression of Rab11A fused to a mCherry tag is
127 under the control of an N-terminal ddFKBP tag, which allows regulation of
128 recombinant protein levels by the inducer Shield-1. Using super-resolution live
129 imaging of parasites expressing the Inner Membrane Complex protein IMC3-YFP and
130 mCherryRab11A-WT, we clearly observed bi-directional trajectories of Rab11A-
131 positive vesicles between the basal and the apical poles of the parasite both, within the
132 parasite cytosol (Fig 1C and Suppl. Movie SM1) and along the parasite cortex
133 delineated by the IMC3-YFP staining (Fig 1C and Suppl. Movie SM2). We also
134 confirmed by videomicroscopy the enrichment of Rab11A at the Golgi/ELC area of

135 newly formed daughter cells and the transport of Rab11A vesicles along the daughter
136 bud scaffold (Suppl. Movie SM3). Interestingly, we also noticed Rab11A-positive
137 dynamic vesicles and tubular structures in the residual body region (Fig 1C, RB). This
138 region has been recently described to harbor a dense actino-myosin network that
139 interconnects the intracellular dividing tachyzoites [6] [7], suggesting that Rab11A
140 may regulate actin-dependent material exchanges between the parasites or the
141 dynamics of this cell-to-cell connecting network. In line with this observation, after
142 transient expression of actin chromobodies coupled to Emerald GFP (Cb-E) that
143 specifically label filamentous actin [7], we visualized Rab11A-positive vesicles
144 moving along actin-positive structures at the parasite cortex (Fig. 1D, upper panel and
145 Suppl. Movie SM4) or anchored to dynamic F-actin structures within the parasite
146 cytosol (Fig. 1D, lower panel and Suppl. Movie SM5). As previously observed [7],
147 we also detected very dynamic F-actin structures at the Golgi/ELC area that co-
148 distribute with the Rab11A signal (Suppl. Movie SM4), suggesting that vesicle
149 budding and/or transport from these compartments may depend on the actin
150 cytoskeleton. To investigate whether Rab11A-positive vesicle movements depend on
151 the actin cytoskeleton, we treated IMC3-YFP / mcherryRab11A-WT tachyzoites with
152 cytochalasin D (CD) for 30 minutes before recording parasites by live imaging.
153 Depolymerizing actin filaments by CD prevented vesicle trafficking and led to the
154 formation of *quasi* static cytosolic and cortical Rab11A-positive clusters (Fig 1E,
155 Suppl. Movie SM6).

156 Collectively, these data demonstrated that Rab11A-positive vesicle movement is
157 dependent on the actin cytoskeleton activity and that Rab11A might participate in (i)
158 vesicle budding from the TGN/ELC, (ii) cargo transport between the apical and basal
159 poles of the parasite and (iii) material exchange between the replicating parasites via
160 release of vesicles at the basal pole.

161

162 **Rab11A-positive vesicles dynamically co-distribute with DG**

163 The DG-mediated secretory pathway is considered in *T. gondii* to be the default
164 constitutive secretory pathway based on the observation that the soluble SAG1 protein
165 truncated of its GPI anchor (SAG1ΔGPI) is transported within DGs before being
166 released into the vacuolar space [10] [31]. Interestingly, the dynamic motion of
167 Rab11A-positive vesicles was very similar to the recently described actin and myosin

168 F-dependent movements of DGs [31] and Rab11A is a known regulator of exocytosis
169 in other eukaryotic systems [14].

170 In order to explore dense granule dynamics in relation to Rab11A, we expressed
171 SAG1ΔGPI-GFP in mcherryRab11A-WT parasites. Using live imaging, we
172 confirmed that the DG content was efficiently released as illustrated by the
173 localization of the GFP signal into the vacuolar space (Fig 2A). The GFP-positive
174 DGs detected in the parasite cytosol displayed a significant and dynamic co-
175 distribution with mcherryRab11A-WT positive vesicles (Fig 2B, 2C). 33,7% of the
176 DG population co-distributed over time with Rab11A-positive vesicles in replicating
177 tachyzoites, while 26,1% of Rab11A-positive vesicles co-distribute with DGs. In
178 agreement, the fluorescent signal intensity profile indicates that GFP-positive DG and
179 mcherryRab11A-positive vesicles are closely apposed (Fig 2A and 2B). This is also
180 clearly visualized in the movie SM7 (Fig 2D), in which a DG appeared docked onto a
181 Rab11A-positive vesicle, the latter being anchored at the periphery of the parasite,
182 and both compartments are simultaneously transported along the parasite cortex (Fig
183 2D). We tracked this GFP-positive DG motion (Fig 2E and 2F; Suppl. Movies SM8
184 and SM9) and fitted the recorded xy positions over time using mathematical models
185 of “directed” or “diffusive” motion (see M&M) [32]. We confirmed that the DG
186 trajectory 2 is consistent with a “directed” motion (fitted curve, Fig 2F), characteristic
187 of a vesicle moving along cytoskeleton tracks, in contrast to the trajectories 1 and 3,
188 consistent with “confined diffusive” motions [32]. This result, together with the
189 inhibition of Rab11A-positive vesicle (Fig 1D) and DG [31] movements upon CD
190 treatment, strongly suggests that Rab11A promotes DG transport by mediating DG
191 tethering along actin filaments, at least at the parasite cortex.

192

193 **Rab11A promotes DG exocytosis**

194 To assess whether Rab11A regulates DG transport, docking or the later step of fusion
195 at the PM, we used a previously established parasite strain that over-expresses in a
196 rapidly inducible manner an inactive GDP locked version of Rab11A fused to the
197 mCherry fluorescent reporter (DDmCherrycmycRab11A-DN-RHΔKu80; from here
198 called mCherryRab11A-DN and distinguished from mCherryRab11A-WT) [27] [30].
199 By WB, we confirmed that both Rab11A-WT and Rab11A-DN proteins were
200 expressed in similar amounts after 4 h induction with Shield-1 (Fig 3A). First, we

201 monitored DG release in fixed Rab11A-WT and Rab11A-DN intracellular tachyzoites
202 following gentle saponin permeabilization, which improved detection of secreted
203 GRA proteins localized in the vacuolar space and at the PVM. To rule out any
204 indirect effect of the previously described cytokinesis defect on DG secretion in
205 Rab11A-DN parasites [27], we pre-treated freshly egressed extracellular tachyzoites
206 for 1 h with Shield-1 before seeding them on a fibroblast monolayer and analyzed DG
207 secretion 2h and 4h after parasite invasion (Fig 3B). Our data revealed a highly
208 significant block of GRA1 and GRA3 secretion in Rab11A-DN parasites in contrast
209 to Rab11A-WT in which both proteins were typically released in the vacuolar space
210 or decorated the PVM (Fig 3B and 3C). A similar observation holds for additional
211 GRA proteins (GRA2, GRA5, GRA6 and GRA16) as shown in Suppl. Fig 1. Notably,
212 in contrast to Rab11A-WT parasites, GRA16-positive DGs were also retained within
213 Rab11A-DN parasite cytosol and accordingly GRA16 no longer reached the host cell
214 nuclei 16h post-infection [33] (Suppl. Fig 1B).

215 To further analyze the role of Rab11A in DG secretion, we also expressed
216 SAG1ΔGPI-GFP in mcherryRab11A-DN parasites. In contrast to Rab11A-WT
217 parasites, Rab11A-DN parasites were drastically impaired in their ability to release
218 SAGΔGPI-GFP into the PV space (Fig 3D). Consequently, DGs were densely packed
219 in the cytosol, which impaired reliable automatic tracking of all vesicles and therefore
220 the quantification of the percentage of directed *versus* diffusive trajectories in the total
221 DG population. Nonetheless, DGs appeared to mostly display normal diffusive and
222 confined motions (Fig 3F and Suppl. Movie SM10). In particular, the accumulation of
223 DGs observed at the altered interface between the two segregating daughter cells
224 accounted for a local *quasi* static behavior as illustrated by their confined trajectories
225 (Fig 3F: trajectories 2, 3 and Suppl. Movie SM10). Few longer-range trajectories
226 could be detected along the cortex of the parasites (such as illustrated for trajectory 1),
227 however they never fitted a model of directed motion with good probability. In
228 support of this result, analysis of cortical DG trajectories in Rab11A-WT and
229 Rab11A-DN parasites revealed a significant increase in the coefficient of diffusion of
230 Rab11A-DN trajectories, suggesting a role for Rab11A in regulating DG directed
231 transport along the parasite cortical cytoskeleton (Fig 3G). Finally, we performed an
232 experiment in which we washed out 0.5μM- (SM11) or 1μM- (SM12) Shield-1 pre-
233 induced Rab11A-DN parasites in order to stop the expression of the Rab11A-DN

234 protein. 4h after Shield-1 removal, we clearly observed a strong accumulation of
235 GFP-positive DGs at the PM separating dividing parasites together with the re-
236 initialization of their content release (Suppl. Movies SM11 and SM12). Since this PM
237 accumulation was not detected in Rab11A-DN parasites in presence of Shield-1, this
238 suggests that Rab11A is required for the early step of DG docking/tethering at the
239 PM. Of note, as vesicle docking/tethering precedes the final fusion step of the
240 exocytic process, we could not decipher whether Rab11A is also involved in the
241 fusogenic process itself.

242 Collectively, our data indicate that Rab11A regulates both the directed transport of
243 DG along cytoskeleton tracks (Fig 1D and Fig 2D, E, F) and their exocytosis in the
244 PV space likely by promoting DG docking/tethering at the parasite PM.

245

246 **Rab11A regulates transmembrane protein localization at the PM**

247 Based on our previous study [27], we proposed that Rab11A is required for the
248 delivery of vesicles containing SAG1 and probably other surface proteins, from the
249 endosomal network to the plasmalemma of daughter cells, where new PM is
250 synthesized, similar to the function described in other eukaryotes. This prompted us to
251 investigate whether Rab11A might regulate the localization of other surface proteins
252 in *T. gondii* during replication. We transiently transfected Rab11A-WT and Rab11A-
253 DN parasites with plasmids encoding the transmembrane HA-tagged Glucose
254 transporter 1 (GT1) [34] or the Ty-tagged rhomboïd protease 4 (ROM4) [35]. In
255 contrast to the rhomboid protease ROM1 that localizes to micronemes, ROM4 was
256 found to be targeted to the tachyzoite PM, suggesting that it may be transported
257 through the constitutive pathway [35] [36]. Similar to DGs, GT1 and ROM4 proteins
258 were retained in intracellular vesicles and were no longer delivered to the parasite PM
259 (Fig 3H). In addition, we took advantage of the impaired exocytosis activity in
260 Rab11A-DN parasites to study whether different populations of secretory vesicles
261 may co-exist during parasite replication. Co-localization studies in fixed parasites
262 showed that ROM4 and GRA3 partially co-localize but were also detected in distinct
263 vesicular compartments both immediately after parasite invasion when de novo
264 synthesis of DG proteins occurs and also after the first division cycle (Suppl. Fig 1C).
265 This may reflect a distinct timing of protein synthesis and vesicle release from the
266 Golgi to the PM but it also suggests the existence of different regulatory pathways for
267 the trafficking of protein localized at the PM *versus* proteins secreted into the

268 vacuolar space. In particular, transmembrane proteins may be actively recycled during
269 parasite division as suggested in a previous study on the retromer subunit TgVPS35
270 [37] and more recently during extracellular parasite motility [38]. Thus, our data
271 indicate a broader role of Rab11A-mediated exocytosis for the delivery of proteins at
272 the PM and for the release of DG proteins into the vacuolar space during parasite
273 replication.

274 Importantly, unlike GRA protein secretion, DG biogenesis was not impaired in
275 Rab11A-DN parasites as assessed by transmission electron microscopy (Fig 4). In
276 addition, supporting a major disturbance in DG exocytosis, the IVN could not be
277 detected in the drastically reduced vacuolar space characterized by the PVM being
278 closely apposed to the parasite PM (Fig 4B and 4C). We also detected the previously
279 described defect in daughter cell membrane segregation [27] (Fig 4C, arrows).

280

281 **Rab11A regulates adhesion and motility of extracellular parasites**

282 A role for Rab11A in parasite invasion has been previously demonstrated [30]. To
283 explore which steps of parasite entry (e.g. adhesion, motility, invasion) were altered,
284 we treated extracellular Rab11A-WT and -DN parasites with Shield-1 for 2 h before
285 monitoring their ability to adhere to host cells. We found that Rab11A-DN
286 tachyzoites were severely impaired in their surface attachment to human fibroblast
287 (HFF) monolayers compared to Rab11A-WT parasites (Fig 5A). Furthermore,
288 parasites that successfully adhered exhibited a strong defect in motility as quantified
289 by the percentage of parasites displaying a SAG1-positive trail deposit (Fig 5B).
290 Importantly, compared to Rab11A-WT parasites, the morphology of adherent motile
291 Rab11A-DN parasites was altered, the latter being wider and shorter, losing their
292 typical arc shape (Fig 5C). Analysis of individual parasites imaged by Scanning EM
293 (n=70 for WT and DN) confirmed that Rab11A-DN parasites display a significant
294 increase in their circularity and accordingly, a decrease in their aspect ratio (AR:
295 major axis/minor axis) (Fig 5C). However, the apical conoid with the emerging
296 microtubule array could be visualized, suggesting no defect in the establishment of
297 parasite polarity (Fig 5C). An impaired recruitment of late glideosome components at
298 the daughter cell buds has been previously reported in dividing Rab11A-DN parasites
299 [27] and could account for the motility defect. However, we induced Rab11A-DN
300 protein expression in non-dividing extracellular parasites and accordingly we did not
301 observe any significant defect in the localization of GAP45 and Myosin Light Chain 1

302 (MLC1) at the parasite cortex of extracellular parasites (Suppl. Fig 2). This indicates
303 that the morphological defect observed in Rab11A-DN parasites is not correlated with
304 a significant perturbation of glideosome component localization.

305 The microneme protein MIC2, a transmembrane protein released at the PM of the
306 parasite, promotes parasite adhesion and motility [39] [40]. First, we confirmed by
307 IFA that MIC2-positive micronemes were detected at the apical pole of extracellular
308 induced Rab11A-DN parasites, indicating no major defect in their localization (Suppl.
309 Fig 3A). Secretion of microneme proteins by extracellular parasites can be triggered
310 by ethanol, a step followed by their release from the parasite PM after cleavage by
311 proteases. Notably, ROM4 has been shown to promote MIC2 trimming at the parasite
312 PM. Since ROM4 was no longer present at the PM of replicative Rab11A-DN
313 parasites, we investigated whether a similar defect could be observed in 2h Shield-1
314 induced extracellular Rab11A-DN. As previously observed for glideosome
315 components, ROM4 localization at the PM was not perturbed in extracellular induced
316 Rab11A-DN parasites (Suppl. Fig 3B). Next, we performed excretion/secretion assays
317 to assess the transport of MIC2 protein to the parasite PM and its subsequent release
318 in the culture medium. Western blot quantification of the Excreted-Secreted Antigen
319 (ESA) fractions demonstrated a significant reduction in MIC2 release upon induction
320 of microneme exocytosis. Accordingly, a slight increase in MIC2 protein level was
321 observed in the pellet fraction, also indicating that the observed decrease in MIC2
322 secretion is not due to a defect in protein synthesis. As observed by IFA, a reduced
323 level of constitutive GRA1 secretion was also detected by WB, which correlates with
324 GRA1 accumulation in the parasite pellet fraction (Fig 5D and 5E). Thus, our data
325 suggest that the defect of extracellular Rab11A-DN parasites in host cell adhesion and
326 motility MIC2 are at least partially due to an impairment of efficient MIC2 delivery to
327 the PM.

328 Lastly, Rab11A-DN parasites that successfully adhered to the surface of host cells,
329 displayed only a mild defect in host cell invasion (Fig 5F). This was supported by the
330 observation of a correctly formed RON4-positive junction by invading Rab11A-DN
331 parasites (Fig 5F).

332 Collectively, our results demonstrate that Rab11A promotes parasite invasion by
333 regulating parasite adhesion and motility, but not the formation of the circular

334 junction. This defect correlates with severe morphological alterations of extracellular
335 parasites.

336

337 **Rab11A-positive vesicles accumulate at the apical pole during parasite motility** 338 **and host cell invasion**

339 The active role of Rab11A in parasite adhesion and motility led us to explore the
340 localization of Rab11A in motile extracellular and invading parasites. Live imaging of
341 mcherryRab11A-WT revealed an unexpected polarized motion of Rab11A-positive
342 vesicles towards two main foci localized at the apical tip of extracellular adhering and
343 motile parasites (Fig 6A, Suppl. Movie SM13). This process appeared to be prolonged
344 during host cell invasion (Fig 6B, SM14). This Rab11A apically polarized
345 localization in invading parasites was further confirmed in fixed parasites after
346 labeling of the circular junction using the RON4 marker (Fig 6C).

347

348 **Rab11A regulates polarized secretion of DG content during parasite motility and** 349 **host cell invasion**

350 Next, we assessed whether Rab11A regulates the secretion of DGs, not only during
351 parasite replication (Fig 3) but also during parasite motility and invasion. Similarly to
352 our live imaging data (Fig 6), we found a clear localization of Rab11A at two foci
353 localized at the apex of extracellular parasites that have been allowed to move on
354 coverslips prior fixation (Fig 7A). These Rab11A foci strongly co-localized with the
355 DG protein GRA1, suggesting that the apically polarized secretion of DGs may play a
356 role in the regulation of parasite adhesion and motility. A similar co-recruitment of
357 both, Rab11A and DG at two apical foci was observed during host cell invasion (Fig
358 7B). Most importantly, we observed a complete inhibition of this polarized secretion
359 of DG in extracellular motile induced Rab11A-DN parasites (Fig 7A) and during host
360 cell invasion (Fig 7B). This result demonstrates that Rab11A regulates the apically
361 polarized secretion of DGs during the early steps of parasite adhesion and entry into
362 host cells. This apical DG secretion may reflect the delivery of a new membrane pool
363 or regulatory factors contributing to parasite motility.

364

365 **Discussion**

366 In this study, we unraveled an essential role of Rab11A in the delivery of

367 transmembrane proteins at the parasite PM and the release of DG proteins into the
368 vacuolar space.

369 In other eukaryotic systems, Rab11A localizes to the endocytic recycling
370 compartment (ERC) and has been implicated in the trafficking of internalized
371 receptors from the ERC to the PM [8]. Rab11A also localizes to the TGN
372 compartment, where it regulates transport of material from this compartment to the
373 ERC or the PM [16]. Similarly, during *T. gondii* cytokinesis, Rab11A localizes to the
374 Golgi/ELC region of daughter cells, and at the tip of growing buds, suggesting a
375 polarized transport of *de novo* synthesized material between these two locations
376 during daughter cell emergence. Interestingly, such apically polarized localization of
377 Rab11A was also evident during extracellular parasite adhesion and motility. Thus,
378 one may envision that components of the apical complex, a microtubule-rich structure
379 from which emanates the subpellicular microtubules [41], may control Rab11A-
380 dependent recruitment and exocytosis of specific cargos at the apical pole of the
381 parasite. In particular, RING2, a component of the apical polar ring, was shown to
382 function in constitutive and cGMP-stimulated secretion of microneme proteins [42].
383 More recently, two other components of the apical polar ring, APR1 and the Kinesin
384 A, were also reported to regulate MIC2 secretion [42]. Hence, it will be of interest to
385 investigate whether Rab11A could also interact with components of the apical polar
386 ring to promote exocytosis of micronemes and DG content during extracellular
387 motility.

388

389 Moreover, during the G1 phase of the cell cycle, videomicroscopy recordings of
390 mCherryRab11A-WT expressing parasites revealed highly dynamic Rab11A-positive
391 vesicles displaying bidirectional trajectories between the apical and the basal poles,
392 with a pronounced accumulation at the basal pole of the parasite, consistent with this
393 location being a preferential site for exocytic events. In line with this, the double
394 membrane of the IMC may be considered a major physical barrier for internalization
395 and secretion of material at the parasite plasma membrane. Therefore, it is possible
396 that exocytic events may be enhanced at sites where the IMC interrupts, e.g. at the
397 apical and basal ends of the parasite. In agreement, previous studies showed massive
398 exocytosis of the DG protein GRA2 in multi-lamellar vesicles at the basal pole of the
399 parasite shortly after entry [43]. We also observed Rab11A-positive vesicles and
400 tubular structures in the region of the residual body, which interconnects parasites

401 during intracellular replication. This region was recently reported to harbor a dense
402 actin-myosin network that connects the parasites within the PV ensuring synchronous
403 divisions [6] [7]. Thus, Rab11A- and actin-dependent vesicular transport may regulate
404 exchanges between parasites within the vacuole. Alternatively, Rab11A may also
405 contribute to the regulation of the actin network function and dynamics. Indeed, in
406 plants, it has been shown that dysregulated Rab11A activity affects actin organization
407 in the apical region of growing pollen tubes [44]. Supporting the hypothesis of a
408 specific interaction between Rab11A and the actino-myosin cytoskeleton in vesicle
409 transport, depolymerizing actin filaments results in the formation of *quasi* static
410 cytoplasmic and cortical Rab11A-positive vesicle clusters. A role for the complex
411 Myosin Vb-FIP2-Rab11A in promoting actin-mediated transport of vesicles has been
412 previously observed in mammalian cells [45] [46] [47]. So far, no homologues of
413 Rab11-family interacting proteins (FIPs) have been identified in *T. gondii* and
414 *Plasmodium*. Nonetheless, *P. falciparum* Rab11A was found to directly interact with
415 the myosin light chain 1 (MLC1/MTIP), which therefore links Rab11A-mediated
416 vesicular transport to unconventional myosins and the actin cytoskeleton [27]. In line
417 with this, over-expression in *T. gondii* of a dominant negative form of myosin A led
418 to similar defects in the completion of cytokinesis, as found when Rab11A-DN is
419 over-expressed [27]. However, as actin depolymerization resulted in the formation of
420 both cytosolic and peripheral Rab11A-positive static vesicles, it is possible that
421 distinct myosins regulate different steps of Rab11A/DG transport e.g. MyoF in the
422 cytosol and from the TGN [31], MyoA at the parasite cortex where the glideosome is
423 located [27], and MyoJ in the cell-to-cell connecting network [6]. Further studies
424 using parasite strains deleted for these molecular motors will address this question.

425

426 Moreover, co-distribution studies indicated that Rab11A-positive vesicles associate
427 with dense granules in a dynamic manner. However, we did not observe Rab11A at
428 the limiting membrane of DG. Rather, these two compartments appear to transiently
429 dock one with each other enabling joint transient motions that were particularly
430 evident at the cortex of the parasite. Indeed, tracking of the trajectories of Rab11A-
431 positive vesicles and DG revealed that Rab11A-positive vesicles promoted DG
432 anchoring at the parasite cortex and their rapid “directed” transport. This mode of
433 transport called “hitchhiking” has been recently described in different cell types and
434 has emerged as a novel mechanism to control organelle movement [48]. During this

435 process, the “hitchhiker” benefits from distinct molecular motors present at the
436 surface of the “vehicle”. This mode of transport may have additional advantages for
437 the hitchhiker. Notably, endosomes represent multifunctional platforms that receive
438 specific signals and could drive the transport of hitchhiker cargo to particular regions
439 of the cell. Also, co-movement of cargo may facilitate interactions at membrane
440 contact sites important for organelle maturation, fusion and/or material exchange.
441 Related to this last aspect, we found that over-expression of Rab11A-DN led to a
442 complete block in DG secretion, which indicates an additional role of Rab11A in
443 vesicle tethering at- and possibly fusion with- the PM. Rab11A is known to promote
444 vesicle tethering and fusion at the PM via its interaction with the exocyst complex in
445 other Eukaryotic systems [14]. However, homologues of the different exocyst
446 complex subunits could not be identified in *T. gondii* [49]. Thus, unexplored
447 mechanisms of Rab11A-mediated vesicle fusion likely exist in *T. gondii*.

448

449 Benefiting from the fast and efficient induction of the Rab11A-DN protein expression
450 in extracellular parasites, we confirmed the previously described defect in host cell
451 invasion [29]. Of note, our numerous attempts to generate parasites expressing C-
452 terminal tagged Rab11A failed, and notably, our attempts to apply the fast inducible
453 AID knock-down system also failed [50]. This is likely due to the fact that the C-
454 terminal domain of the Rabs contains one or two cysteines recognized by
455 geranylgeranyl-transferases to induce their isoprenylation, a modification required for
456 their association with vesicle membranes. The impaired cell invasion of Rab11A-DN
457 expressing parasites results from a strong defect in parasite adhesion to host cells .
458 Indeed, parasites that successfully adhered to host cells were only mildly perturbed in
459 host cell entry. In addition, the secretion of MIC2, an adhesin essential for parasite
460 adhesion and motility was reduced upon dysregulation of Rab11A activity. Secretion
461 of the GPI-anchored protein SAG1 is also altered in Rab11A-DN expressing parasites
462 [27]. Thus, it is likely that the altered secretion of these two host cell adhesins
463 contributes to the decrease in adhesion and motility of Rab11A-DN parasites. In line
464 with a role of Rab11A in the regulation of surface protein trafficking, we also found a
465 strong defect in the localization of the romboïd protease ROM4 and the glucose
466 transporter GT1 at the PM, indicating a broader role of Rab11A in exocytosis. It is
467 likely that distinct exocytic pathways exist in *T. gondii*, such as described in other
468 organisms. In particular, whether a distinct endosome recycling compartment is

469 present in *T. gondii* requires further exploration. Previous studies highlighted that *T.*
470 *gondi* has functionally repurposed its endocytic system to serve the secretory pathway
471 of this fast replicating intracellular parasite [51] [52]. In this context, the TGN appears
472 to be a hybrid compartment to which the endosomal markers (Rab5 and Rab7) are
473 tightly associated [52]. Therefore, one may envision that material internalized from
474 the PM reaches this hybrid TGN/ELC compartment before being re-directed to other
475 target membranes, such as the rhoptries, the PM and the degradative vacuole (VAC).
476 Such a recycling process has been recently observed during extracellular parasite
477 motility [38]. Recycling of mother material during daughter cell emergence may also
478 follow this indirect secretory pathway, while *de novo* synthesized proteins may traffic
479 via the direct TGN to PM route.

480 Finally, exocytosis of DG proteins in *T. gondii* is commonly named the “constitutive
481 secretory pathway” due to continuous release of cargos into the vacuolar space during
482 intracellular replication. However, during extracellular parasite motility and invasion,
483 imaging of both live and fixed parasites revealed an unexpected polarized transport of
484 Rab11A-positive vesicles towards two main foci located just beneath the conoid,
485 where the IMC interrupts. This is consistent with a mechanism of “regulated”
486 secretion triggered upon parasite adhesion to host cells. In mammalian cells, Rab11A-
487 dependent polarized secretion towards the leading edge of motile cells is essential to
488 promote persistent migration [53]. This process provides additional membrane
489 ensuring the extension of the leading edge but also contributes to the translocation of
490 regulators of several signaling pathways, including ones involved in actin and
491 microtubule cytoskeleton activity. In *T. gondii*, the apical exocytosis of some
492 effectors may regulate not only actin-based parasite adhesion and motility but also the
493 modulation of the conoid activity involved in microtubule-dependent motility. Such
494 regulation has been demonstrated for the lysine methyltransferase, AKMT (Apical
495 complex lysine (K) methyltransferase) [54] [55]. Thus, future research will aim to
496 identify the cargos that are apically secreted in a Rab11A-dependent manner and their
497 putative role in regulating parasite motility. We found that some of these factors are
498 likely to be contained in DG as the latter co-localized with Rab11A at the two main
499 apical foci that we observed. Interestingly, it has been recently shown that the DG
500 protein GRA8 contributes to the regulation of parasite motility by regulating conoid
501 extrusion and organization of the microtubule network [56].

502 Therefore, identifying Rab11A interactors will be an important future goal, as it will
503 improve our understanding of the mechanisms regulating the distinct exocytic
504 pathways in *T. gondii*. In particular, it will be important to characterize the molecular
505 mechanisms involved in Rab11A-positive vesicle anchoring to actin or microtubule
506 molecular motors, and of vesicle tethering and fusion with the PM both, during
507 parasite motility and intracellular replication. Finally, exploring a putative functional
508 interaction between Rab11A-dependent secretion and the apical complex may lead to
509 the discovery of novel regulated secretory mechanisms essential to ensure parasite
510 virulence.

511

512 **Materials and Methods**

513 **Parasite culture and transfection**

514 *Toxoplasma gondii* Type I RH Δ KU80 Δ HXGPRT parasites were grown on confluent
515 Human Foreskin Fibroblast (HFF) cells (CCD-1112Sk (ATCC, CRL-2429TM)) which
516 were cultured in complete DMEM (gibcoLife Technologies) supplemented with 10%
517 Fetal Bovine Serum (GibcoLife Technologies) and 1% Pen Strep (gibcoLife
518 Technologies). To obtain the transgenic parasites, the RH Δ KU80 Δ HXGPRT parental
519 strain was transfected by electroporation following standard procedures with 50 μ g of
520 the following plasmids.

Plasmid	Selection	Laboratory
DD-cmycmcherry-Rab11A-WT	HXGPRT	Meissner M [26]
DD-cmycmcherry-Rab11A-DN	HXGPRT	Meissner M [26]
IMC3-YFP	DHFR	Gubbels MJ
SAG1 Δ GPI-GFP	CAT	Heaslip A [31]
pLic GRA16-HA	DHFR	MA Hakimi [33]

521 Following transfection, parasites were subjected to drug selection and verified for the
522 transfection efficiency by immunofluorescence analysis. Subsequently the parasites
523 were subjected to cloning by serial dilution.

524 **Production of the anti-TgRab11A antibodies**

525 Recombinant purified GST-Rab11A protein was used to raise a *TgRab11A* specific
526 mouse polyclonal antibody. The cleavage site present between the GST tag and
527 Rab11A was digested with Precision protease (GE life science). GST-Rab11A bound
528 to agarose beads was washed with 10 bed volumes of Cleavage buffer (50mM Tris
529 HCl, pH7.0, 150mM NaCl, 1mM EDTA, 1mM DTT) at 4°C. Precision protease (40
530 units) was added to the cleavage buffer and incubated with the beads at 4°C
531 overnight. The purified Rab11A was collected in the supernatant. 50µg of the purified
532 recombinant protein suspended in Freund's Adjuvant were injected intra-peritoneally
533 into mice over a series of 4 boosts. Following the third boost, a sample of serum was
534 collected and tested by western blot for antibody reactivity using a total protein
535 extract of parasites. Once specific antibody activity was detected mice were sacrificed
536 and serum collected and stored at -20°C.

537

538 **Protein sample preparation and Western Blot**

539 Parasites were lysed in lysis buffer (NaCl 150mM, TrisHCl 20mM, EDTA 1mM, 1%
540 TritonX100, protease inhibitors) and total proteins were subjected to electrophoresis
541 in a 10% polyacrylamide gel. The proteins were transferred onto a nitrocellulose
542 membrane (Amersham™Protran™ 0.45µ NC) by a standard western blot procedure.
543 The membrane was blocked with 5% milk (non-fat milk powder dissolved in TNT
544 buffer: 100mM Tris pH8.0, 150mM NaCl and 0.1% Tween20) and probed with the
545 indicated primary antibodies followed by species-specific secondary antibodies
546 conjugated with HRP. The probed nitrocellulose membranes were visualized using
547 the ECL Western blotting substrate (Pierce).

548

549 **Immunofluorescence assay**

550 Confluent HFF monolayers were grown on coverslips and infected with parasites
551 prior to fixing with 4 % PFA for 15 min. After quenching with 50mM NH₄Cl, the
552 coverslips were permeabilized with 0.2% triton dissolved in 5% FBS-PBS for 30 min.
553 Coverslips were incubated with primary antibodies in 0.1% triton dissolved in 2%
554 FBS-PBS and then washed thrice with 1X PBS. Alternatively, the coverslips were
555 incubated with primary antibodies in 0.01% Saponin diluted in 2%FBS-PBS for 1 h.
556 Incubation with secondary antibodies was performed in 0.1% triton or 0.01% Saponin
557 dissolved in 2%FBS-PBS for 30 min. To label invading parasites, freshly egressed

558 extracellular parasites expressing Rab11A-WT and Rab11A-DN were induced with
559 Shield-1 for 2 h and seeded onto HFF monolayers in a 24-well plate at a concentration
560 of 2×10^6 parasites (Rab11A-WT) and 4×10^6 (Rab11A-DN) / 500 μ l complete medium
561 containing Shield-1 per coverslip. The plate was centrifuged for 2 min at 1000rpm at
562 room temperature to trigger adhesion and synchronized invasion events. The plate
563 was immediately shifted to a water bath at 37°C and the parasites were fixed with 4%
564 PFA-sucrose at the following time points - 0, 2 and 5 min. Coverslips were washed
565 with PBS and adherent or invading parasites labeled without permeabilization with
566 the anti-SAG1 antibody and a secondary anti-mouse AlexaFluor405 antibody. After
567 washing with PBS, parasites were permeabilized with 0.05% saponin for 10 min,
568 followed by a blocking step with 5% FBS-PBS for 30 min. Next, coverslips were
569 incubated with rabbit anti-RON4 antibodies and secondary anti-rabbit AlexaFluor488
570 to label the circular junction. Depending on the experiment, additional primary
571 antibodies were added to detect GRA1, GRA3 and TgRab11A during parasite
572 invasion. Images were acquired using a Zeiss LSM880 confocal microscope equipped
573 with an airyscan module. Antibodies used for IFA experiments were: rabbit anti-HA
574 (Cell Signaling Technology), rat anti-cMyc (Abcam), mouse anti-SAG1 (our lab),
575 rabbit anti-GAP45 (D. Soldati-Favre), mouse anti-MIC2 (V. Carruthers), mouse anti-
576 ROP 2–4 (JF. Dubremetz), mouse anti-GRA2 (Biotem), mouse anti-GRA5 (Biotem),
577 mouse anti-GRA1 (Biotem), rabbit anti-GRA3 (JF. Dubremetz), rabbit anti-IMC3
578 (MJ Gubbels), rabbit anti-RON4 (M. Lebrun), mouse anti-TY (D. Soldati-Favre) and
579 mouse anti-Rab11A (this study).

580

581 **Invasion assay**

582 Freshly egressed extracellular parasites expressing Rab11A-WT and Rab11A-DN
583 were harvested and treated for 2 h with 1 μ M of Shield-1. Induced parasites were
584 counted and seeded onto HFF monolayers in a 24-well plate at a concentration of
585 2×10^6 parasites (Rab11A-WT) or 4×10^6 parasites (Rab11A-DN) / 500 μ l complete
586 medium containing Shield-1 / coverslip. The plate was centrifuged for 2 min at
587 1000rpm at RT to trigger immediate adhesion and synchronized invasion events.
588 Parasites were then shifted to 37°C for 45min. The slips were washed with PBS –
589 three times prior to fixation. Cells were fixed in 4% PFA for 10 min and subjected to
590 a red/green invasion assay. Briefly, adherent external parasites were labeled without
591 permeabilization with mouse anti-TgSAG1 antibodies, followed by secondary anti-

592 mouse antibodies coupled to Alexa488. After cell permeabilization with Triton 0.1%,
593 invaded intracellular parasites were detected using rabbit anti-TgGAP45 antibodies
594 followed with a secondary anti-rabbit antibodies coupled to Alexa594. All parasites
595 labeled green-red were considered as extracellular, while parasites exclusively red
596 (positive for GAP45) were considered intracellular. At least 300 parasites were
597 counted for each condition performed in triplicate. Data represent mean values \pm SEM
598 from three independent biological experiments.

599

600 **Motility (Trail deposition) Assay**

601 Glass slides were coated with 100 μ g/ml BSA-PBS and incubated at 37°C for 1 h. The
602 slides were washed three times with PBS and allowed to dry. Freshly egressed
603 extracellular Rab11A-WT and Rab11A-DN expressing parasites were harvested and
604 treated for 2 h with 1 μ M of Shield-1. Induced parasites were counted and suspended
605 in HHE buffer (HBSS, 10mM HEPES, 1mM EGTA) containing 1 μ M of Shield-1.
606 1*10⁶ (Rab11A-WT) or 2*10⁶ (Rab11A-DN) parasites were seeded per well and
607 incubated for 15 min at 37°C. Parasites were then fixed with 4% PFA in PBS for 10
608 min at RT. A standard IFA protocol was followed wherein primary mouse anti-SAG1
609 antibodies were used followed by goat anti-mouse secondary antibodies conjugated to
610 Alexa Fluor 488. 200 parasites per coverslip were counted for the presence or absence
611 of a SAG1-positive trail. With internal triplicates, the experiment was performed 3-
612 times. Mean values \pm SEM was calculated.

613

614 **Adhesion assay**

615 Freshly egressed extracellular Rab11A-WT and Rab11A-DN parasites were harvested
616 and treated for 2 h with 1 μ M of Shield-1. Parasites were then counted and
617 resuspended in Endo buffer (44.7mM K₂SO₄, 10mM Mg₂SO₄, 100mM sucrose, 5mM
618 glucose, 20mM Tris, 0.35% wt/vol BSA - pH 8.2) containing 1 μ M cytochalasin D
619 and 1 μ M of Shield-1. 2*10⁶ parasites were then seeded onto confluent HFF cells
620 grown on glass coverslips, spun down for 2 min at 1000rpm and incubated for 15 min
621 at 37°C in the presence of 1 μ M Cytochalasin D and Shield-1. The coverslips were
622 washed with PBS before fixation with PFA 4% for 10 min. The Red/Green assay was
623 performed (see “Invasion assay”). Data were compiled from 3 independent
624 experiments after counting 20 fields /coverslip at 60X magnification (done in
625 triplicate for each condition/ experiment). Data collected are mean values \pm SEM.

626

627 **Excreted Secreted Antigens assay**

628 50*10⁶ freshly egressed extracellular Rab11A-WT and Rab11A-DN parasites were
629 harvested and treated for 2 h with 1 μ M of Shield-1. Shield-1 treatment was
630 maintained throughout the experiment in all media. Parasites were mixed with an
631 equal volume of pre-warmed intracellular (IC) buffer (5 mM NaCl, 142 mM KCl, 1
632 mM MgCl₂, 2mM EGTA, 5.6 mM glucose and 25 mM HEPES, pH 7.2) and spun
633 down at 1500rpm, RT for 10 min. The pellet was washed once in the IC buffer under
634 similar conditions and then resuspended in Egress buffer (142 mM NaCl, 5mM KCl,
635 1 mM MgCl₂, 1mM CaCl₂, 5.6 mM glucose and 25 mM HEPES, pH 7.2) containing
636 +/- 2% ethanol and incubated for 30 min at 37°C. The samples were spun down at
637 14000 rpm for 15 min at 4°C and the supernatant containing ESA saved. Pellets were
638 washed once in 1x PBS and saved. The ESA and pellet fractions were suspended in
639 4x Laemelli blue buffer and subjected to Western blot as described above. The blots
640 were probed with mouse anti-MIC2 (V. Carruthers), mouse anti-GRA1 (Biotem) and
641 rabbit anti-eno2 (our lab) antibodies.

642 **Transmission electron microscopy (TEM)**

643 After infection of a confluent HFF monolayer, cells containing replicating shield-1
644 induced Rab11A-WT and Rab11A-DN expressing parasites were detached with a
645 scraper, spun down and fixed with 1% glutaraldehyde in 0.1 M sodium cacodylate pH
646 6.8 overnight at 4°C. Cells were post-fixed with 1% osmium tetroxide and 1.5%
647 potassium ferricyanide for 1 h, then with 1% uranyl acetate for 45 min, both in
648 distilled water at RT in the dark. After washing, cells were dehydrated in graded
649 ethanol solutions then finally infiltrated with epoxy resin and cured for 48 hs at 60°C.
650 Sections of 70–80 nm thickness on formvar-coated grids were observed with a
651 Hitachi H7500 TEM (Elexience, France), and images were acquired with a 1 Mpixel
652 digital camera from AMT (Elexience, France).

653 **Scanning Electron microscopy (SEM)**

654 Parasites were allowed to adhere and move on BSA coated-glass coverslips for 15
655 min at 37°C before being fixed with 2.5 % glutaraldehyde in 0.1 M sodium
656 cacodylate for 30 min. After washing, cells were treated with 1 % osmium tetroxide
657 in water, in the dark for 1 hour. Cells were dehydrated with increasing ethanol
658 concentration baths. After two pure ethanol baths, cells were air-dried with HMDS.
659 Finally, dry coverslips were mounted on stubs and coated with 5 nm platinum
660 (Quorum Technologies Q150T, Milexia, France) and cells were imaged at 2 kV by a
661 secondary electron detector with a Zeiss Merlin Compact VP SEM (Zeiss, France).

662 **Videomicroscopy**

663 Time-lapse video microscopy was conducted in LabTek chambers installed on an
664 Eclipse Ti inverted confocal microscope (Nikon France Instruments, Champigny sur
665 Marne, France) with a temperature and CO₂-controlled stage and chamber (Okolab),
666 equipped with two Prime 95B Scientific Cameras (Photometrics, UK) and a CSU W1
667 spinning disk (Yokogawa, Roper Scientific, France). The microscope was piloted
668 using MetaMorph software (Universal Imaging Corporation, Roper Scientific,
669 France). A live-SR module (Gataca Systems, France) was added to the system to
670 improve the obtained resolutions. Exposure time of 500 ms was used for the
671 simultaneous acquisition of the GFP and mCherry channels, in dual camera mode
672 (with band pass filters 525/50 nm and 578/105 nm, dichroic mirror at 560 nm, and
673 laser excitation at 488 nm and 561 nm). Videos were captured at 2 frames per second
674 (fps).

675 **Automatic Tracking and vesicle co-distribution using the Imaris Software**

676 Automatic tracking of vesicles using the Imaris software (Bitplane, Oxford
677 Instruments) was applied on the recorded videos retrieved from the GFP and mcherry
678 channels of SAGΔGPI-GFP / mcherryRab11A-WT expressing parasites. We first
679 used the tool “Spot detector” for selecting-filtering spot size and intensity values for
680 each channel. Next, we manually removed detection of false GFP-positive spots
681 (notably detected in the vacuolar space due to the secretion of the SAGΔGPI protein
682 in Rab11A-WT parasites). The tool “Track Manager” was used to manually correct

683 the obtained tracks when required and to extract the xy positions of a given spot over
684 time enabling to calculate the Mean Square Displacement (MSD) using MATLAB
685 (see below). The tool “spot co-localization” was used to calculate the percentage of
686 co-distribution between DG and Rab11A-positive vesicles. A distance of 300 nm
687 between the spots was selected corresponding to the average size of the vesicles. At a
688 given time point and for the entire vacuole, the number of all detected green spots, as
689 well as the number of green spots co-distributing with the red spots were extracted to
690 calculate the co-distribution percentage. This was repeated over 5 consecutive time
691 points every 2 s for the first 10 s of recording to avoid bleaching of the fluorescent
692 signals. The mean co-distribution percentage over these 5 time points was calculated
693 per vacuole. The mean +/- SD of 10 vacuoles was then calculated.

694 **Manual Tracking and Mathematical Modeling with MATLAB**

695 When indicated, the manual tracking plugin from the Image J software
696 (<https://imagej.nih.gov/ij/>) was applied on the images obtained with the MetaMorph
697 software to extract in time the spatial xy positions of the fluorescent vesicles. In order
698 to track and model the type of motion of the vesicle, images were processed in
699 MATLAB (www.mathworks.com) by applying *fit* function (‘poly1’ or ‘poly2’
700 options).

701 MSD was calculated thanks to a MATLAB script according to the formula:

$$702 \quad MSD(n\Delta t) = \frac{1}{N-n} \sum_{i=1}^{N-n} (d_{i+n} - d_i)^2$$

703 MSD curves were fitted according to the formula:

704 $MSD = 4Dt + v^2t$ (with D the Diffusion Coefficient and v the velocity), for directed
705 motion

706 $MSD = 4Dt$ (with D the Diffusion Coefficient), for normal diffusion.

707 **Statistics**

708 Means and SEM / SD were calculated in GraphPad (Prism). *P*-values were calculated
709 using the Student's *t*-test assuming equal variance, unpaired samples and using two-
710 tailed distribution.

711 **Acknowledgments**

712 We thank Aoife Heaslip, Marc-Jan Gubbels, Dominique Soldati-Favre, Jean-François
713 Dubremetz, Maryse Lebrun and Ali-Mohamed Hakimi for sharing of reagents. KV,
714 SM and GL have been supported by the Laboratoire d'Excellence (LabEx) ParaFrap
715 from the National Agency for Research ANR-11-LABX-0024 grant and by the ANR-
716 14-CE14-0002-01 grant. SM has been supported by a joint Chaire d'Excellence from
717 University of Lille and the Centre National pour la Recherche Scientifique (CNRS).

718

719 **References**

720

- 721 1. Besteiro S, Dubremetz, JF and Lebrun M. The moving junction of apicomplexan
722 parasites: a key structure for invasion. *Cell. Microbiol.* 2011 ; 13, 797–805.
- 723 2. Dubois DJ, Soldati-Favre D. Biogenesis and secretion of micronemes in *Toxoplasma*
724 *gondii*. *Cell Microbiol.* 2019; 21:e13018.
- 725 3. The triumvirate of signaling molecules controlling *Toxoplasma* microneme
726 exocytosis: Cyclic GMP, calcium, and phosphatidic acid. Bullen HE, Bisio H, Soldati-
727 Favre D. *PLoS Pathog.* 2019; 15:e1007670.
- 728 4. Hakimi MA, Olias P, Sibley LD. *Toxoplasma* Effectors Targeting Host Signaling and
729 Transcription. *Clin Microbiol Rev.* 2017; 30:615-645.
- 730 5. Muñoz-Hernández S, Carmen MG, Mondragón M, Mercier C, Cesbron MF,
731 Mondragón-González SL, González S, Mondragón R. Contribution of the residual
732 body in the spatial organization of *Toxoplasma gondii* tachyzoites within the
733 parasitophorous vacuole. *J Biomed Biotechnol.* 2011; 2011:473983.
- 734 6. Frénal K, Jacot D, Hammoudi PM, Graindorge A, Maco B, Soldati-Favre D.
735 Myosin-dependent cell-cell communication controls synchronicity of division in
736 acute and chronic stages of *Toxoplasma gondii*. *Nat Commun.* 2017; 8:15710.
- 737 7. Periz J, Whitelaw J, Harding C, Gras S, Del Rosario Minina MI, Latorre-Barragan F
738 et al. *Toxoplasma gondii* F-actin forms an extensive filamentous network required for
739 material exchange and parasite maturation. *Elife.* 2017; 6 pii: e24119.

- 740 8. Mercier C, Cesbron-Delauw MF. Toxoplasma secretory granules: one population or
741 more? Trends Parasitol. 2015; 31:604.
- 742 9. Grant BD and Donaldson JG. Pathways and mechanisms of endocytic recycling. Nat
743 Rev Mol Cell Biol. 2009; 10: 597–608.
- 744 10. Striepen B, He CY, Matrajt M, Soldati D, Roos DS. Expression, selection, and
745 organellar targeting of the green fluorescent protein in *Toxoplasma gondii*. Mol
746 Biochem Parasitol. 1998; 92:325-38.
- 747 11. Striepen B, Soldati D, Garcia-Reguet N, Dubremetz JF and Roos DS. Targeting of
748 soluble proteins to the rhoptries and micronemes in *Toxoplasma gondii*. Mol
749 Biochem Parasitol. 2001; 92: 325-338.
- 750 12. Reiss M, Viebig N, Brecht S, Fourmaux MN, Soete M, Di Cristina M, et al.
751 Identification and characterization of an escorter for two secretory adhesins in
752 *Toxoplasma gondii*. J Cell Biol. 2001; 152:563–78.
- 753 13. Stenmark H. Rab GTPases as coordinators of vesicle traffic. Nat Rev Mol Cell Biol.
754 2009; 10:513-25.
- 755 14. Welz T, Wellbourne-Wood J, Kerkhoff E. Orchestration of cell surface proteins by
756 Rab11. Trends Cell Biol. 2014; 24:407-15.
- 757 15. Campa CC and Hirsch E. Rab11 and phosphoinositides: A synergy of signal
758 transducers in the control of vesicular trafficking. Advances in Biological Regulation.
759 2017;63 :132-139.
- 760 16. Chen W, Feng Y, Chen D, Wandinger-Ness A. Rab11 is required for trans-golgi
761 network-to-plasma membrane transport and a preferential target for GDP dissociation
762 inhibitor. Mol. Biol. Cell. 1998; 9:3241-3257.
- 763 17. Delevoye C, Miserey-Lenkei S, Montagnac G, Gilles-Marsens F, Paul-Gilloteaux P,
764 Giordano F et al. Recycling endosome tubule morphogenesis from sorting endosomes
765 requires the kinesin motor KIF13A. Cell Rep. 2014; 6:445-454.
- 766 18. Schuh M. An actin-dependent mechanism for long-range vesicle transport. Nat Cell
767 Biol. 2011; 13:1431-6.
- 768 19. Senye Takahashi S, Kubo K, Waguri S, Yabashi A, Shin HW, Katoh Y, Nakayama
769 K. Rab11 regulates exocytosis of recycling vesicles at the plasma membrane. Journal
770 of Cell Science 2012 125: 4049-4057.
- 771 20. Wu S, Mehta SQ, Pichaud F, Bellen HJ, Quioco FA. Sec15 interacts with Rab11 via
772 a novel domain and affects Rab11 localization in vivo. Nat. Struct. Mol. Biol. 2005;
773 12:879-85.

- 774 21. Fielding AB, Schonteich E, Matheson J, Wilson G, Yu X, Hickson GR et al. Rab11-
775 FIP3 and FIP4 interact with Arf6 and the exocyst to control membrane traffic in
776 cytokinesis. *EMBO J.* 2005; 24:3389-99.
- 777 22. Westlake CJ, Baye LM, Nachury MV, Wright KJ, Ervin KE, Phu L. Primary cilia
778 membrane assembly is initiated by Rab11 and transport protein particle II (TRAPP
779 complex-dependent trafficking of Rabin8 to the centrosome. *Proc. Natl. Acad. Sci. U.
780 S. A.* 2011; 108:2759-64.
- 781 23. Wilson GM, Fielding AB, Simon GC, Yu X, Andrews PD, Hames RS et al. The
782 FIP3-Rab11 protein complex regulates recycling endosome targeting to the cleavage
783 furrow during late cytokinesis. *Mol Biol Cell.* 2005; 16:849–860.
- 784 24. Assaker G, Ramel D, Wculek SK, González-Gaitán M, Emery G. Spatial restriction
785 of receptor tyrosine kinase activity through a polarized endocytic cycle controls
786 border cell migration *Proc. Natl. Acad. Sci. U. S. A.* 2010; 107:22558-63.
- 787 25. Kessler D, Gruen GC, Heider D, Morgner J, Reis H, Schmid KW et al. The action of
788 small GTPases Rab11 and Rab25 in vesicle trafficking during cell migration. *Cell
789 Physiol Biochem.* 2012; 29:647-56.
- 790 26. Kremer K, Kamin D, Rittweger E, Wilkes J, Flammer H, Mahler S et al. An
791 overexpression screen of *Toxoplasma gondii* Rab-GTPases reveals distinct
792 transport routes to the micronemes. *PLoS Pathog.* 2013; 9:e1003213
- 793 27. Agop-Nersesian C, Naissant B, Ben Rached F, Rauch M, Kretzschmar A,
794 Thiberge S et al. Rab11A-controlled assembly of the inner membrane complex is
795 required for completion of apicomplexan cytokinesis. *PLoS Pathog.* 2009;
796 5:e1000270.
- 797 28. Burke JE, Inglis AJ, Perisic O, Masson GR, McLaughlin SH, Rutaganira F et al.
798 Structures of PI4KIII β complexes show simultaneous recruitment of Rab11 and
799 its effectors. *Science.* 2014; 344:1035-8.
- 800 29. McNamara CW, Lee MC, Lim CS, Lim SH, Roland J, Simon O et al. Targeting
801 *Plasmodium* PI(4)K to eliminate malaria. *Nature.* 2013;504:248-253.
- 802 30. Andenmatten N, Egarter S, Jackson AJ, Jullien N, Herman JP, Meissner M.
803 Conditional genome engineering in *Toxoplasma gondii* uncovers alternative
804 invasion mechanisms. *Nat Methods.* 2013;10:125-7
- 805 31. Heaslip AT, Nelson SR, Warshaw DM. Dense granule trafficking in *Toxoplasma
806 gondii* requires a unique class 27 myosin and actin filaments. *Mol Biol Cell.*
807 2016; 27:2080-9.
- 808 32. Wang Y, Jeong Y, Jhiang SM, Yu L, Menq CH. Quantitative characterization of
809 cell behaviors through cell cycle progression via automated cell tracking. *PLoS
810 One.* 2014; 9:e98762

- 811 33. Bougdour A, Durandau E, Brenier-Pinchart MP, Ortet P, Barakat M, Kieffer S,
812 Curt-Varesano A, Curt-Bertini RL, Bastien O, Coute Y, Pelloux H, Hakimi MA
813 Host cell subversion by Toxoplasma GRA16, an exported dense granule protein
814 that targets the host cell nucleus and alters gene expression. Cell Host Microbe.
815 2013; 13:489-500.
- 816 34. Pomel S, Luk FC, Beckers CJM. Host cell egress and invasion induce marked
817 relocations of glycolytic enzymes in *Toxoplasma gondii* tachyzoites. PLoS Pathog.
818 2008; 4:e1000188
- 819 35. Jeffrey S. Buguliskis, Fabien Brossier, Joel Shuman, L. David Sibley. Rhomboid 4
820 (ROM4) Affects the Processing of Surface Adhesins and Facilitates Host Cell
821 Invasion by *Toxoplasma gondii*. PLoS Pathog. 2010; 6: e1000858.
- 822 36. Brossier F, Jewett TJ, Sibley LD, Urban S. A spatially localized rhomboid protease
823 cleaves cell surface adhesins essential for invasion by *Toxoplasma*. Proc Natl Acad
824 Sci U S A. 2005; 102:4146-51.
- 825 37. Sangaré LO, Alayi TD, Westermann B, Hovasse A, Sindikubwabo F, Callebaut I,
826 Werkmeister E, Lafont F, Slomianny C, Hakimi MA, Van Dorsselaer A, Schaeffer-
827 Reiss C, Tomavo S. Unconventional endosome-like compartment and retromer
828 complex in *Toxoplasma gondii* govern parasite integrity and host infection. Nat
829 Commun. 2016; 7:11191.
- 830 38. Gras S, Jimenez-Ruiz E, Klinger CM, Schneider K, Klingl A, Lemgruber L, Meissner
831 M. An endocytic-secretory cycle participates in *Toxoplasma gondii* in motility. PLoS
832 Biol. 2019; 17:e3000060.
- 833 39. Gras S, Jackson A, Woods S, Pall G, Whitelaw J, Leung JM, Ward GE et al. Parasites
834 lacking the micronemal protein MIC2 are deficient in surface attachment and host
835 cell egress, but remain virulent in vivo. Wellcome Open Res. 2017; 2:32.
- 836 40. Whitelaw JA, Latorre-Barragan F, Gras S, Pall GS, Leung JM, Heaslip A et al.
837 Surface attachment, promoted by the actomyosin system of *Toxoplasma gondii* is
838 important for efficient gliding motility and invasion. BMC Biol. 2017; 15:1.
- 839 41. Leung JM, He Y, Zhang F, Hwang YC, Nagayasu E, Liu J et al. Stability and
840 function of a putative microtubule-organizing center in the human parasite
841 *Toxoplasma gondii*. Mol Biol Cell. 2017; 28: 1361–1378
- 842 42. Katris NJ, van Dooren GG, McMillan PJ, Hanssen E, Tilley L, Waller RF. The
843 apical complex provides a regulated gateway for secretion of invasion factors in
844 *Toxoplasma*. PLoS Pathog. 2014; 10:e1004074.
- 845 43. Sibley LD, Niesman IR, Parmley SF, Cesbron-Delauw MF. Regulated secretion
846 of multi-lamellar vesicles leads to formation of a tubulo-vesicular network in

- 847 host-cell vacuoles occupied by *Toxoplasma gondii*. J Cell Sci. 1995; 108:1669-
848 77.
- 849 44. de Graaf BH, Cheung AY, Andreyeva T, Levasseur K, Kieliszewski M, Wu HM.
850 Rab11 GTPase-Regulated Membrane Trafficking Is Crucial for Tip-Focused
851 Pollen Tube Growth in Tobacco. Plant Cell. 2005; 17:2564–2579.
- 852
- 853 45. Horgan CP, McCaffrey MW. The dynamic Rab11-FIPs. Biochem Soc Trans. 2009;
854 37:1032-6.
- 855 46. Chu BB, Ge L, Xie C, Zhao Y, Miao HH, Wang J et al. Requirement of Myosin
856 Vb-Rab11a-Rab11-FIP2 Complex in Cholesterol-regulated Translocation of NPC1L1
857 to the Cell Surface J Biol Chem. 2009; 284: 22481–22490
- 858 47. Schafer JC, Baetz NW, Lapierre LA, McRae RE, Roland JT, Goldenring JR. Rab11-
859 FIP2 Interaction with MYO5B Regulates Movement of Rab11a-Containing
860 Recycling Vesicles. Traffic. 2014; 15: 292–308
- 861 48. Salogiannis J, Reck-Peterson SM. Hitchhiking: A Non-Canonical Mode of
862 Microtubule-Based Transport. Trends Cell Biol. 2017; 27: 141–150.
- 863 49. Tomavo S, Slomianny C, Meissner M, Carruthers VB. Protein trafficking through the
864 endosomal system prepares intracellular parasites for a home invasion. PLoS Pathog.
865 2013; 9:e1003629.
- 866 50. Brown KM, Long S, Sibley LD. Conditional Knockdown of Proteins Using
867 Auxin-inducible Degron (AID) Fusions in *Toxoplasma gondii*. Bio Protoc. 2018;
868 8.pii: e2728
- 869 51. Venugopal K, Marion S. Secretory organelle trafficking in *Toxoplasma gondii*: A
870 long story for a short travel. Int J Med Microbiol. 2018; 308:751-760.
- 871 52. Venugopal K, Werkmeister E, Barois N, Saliou JM, Poncet A, Huot L,
872 Sindikubwabo F, Hakimi MA, Langsley G, Lafont F, Marion S. Dual role of the
873 *Toxoplasma gondii* clathrin adaptor AP1 in the sorting of rhoptry and microneme
874 proteins and in parasite division. PLoS Pathog. 2017; 13:e1006331.
- 875 53. Fletcher SJ, Rappoport JZ. Moving forward: polarised trafficking in cell migration.
876 Trends Cell Biol. 2010; 20:71–78.
- 877 54. Heaslip AT, Nishi M, Stein B, Hu K. The motility of a human parasite,
878 *Toxoplasma gondii*, is regulated by a novel lysine methyltransferase. PLoS
879 Pathog. 2011; 7:e1002201
- 880 55. Stadler RV, White LA, Hu K, Helmke BP, Guilford WH. Direct measurement of
881 cortical force generation and polarization in a living parasite. Mol Biol Cell. 2017;
882 28:1912-1923.

883 56. Díaz-Martín RD, Mercier C, Gómez de León CT, González RM, Pozos SG, Ríos-
884 Castro E et al. The dense granule protein 8 (GRA8) is a component of the sub-
885 pellicular cytoskeleton in *Toxoplasma gondii*. *Parasitol Res.* 2019; 118:1899-1918.

886

887

888

889 **Figure legends**

890 **Figure 1**

891 **A-**Western blot analysis with specific anti-Rab11A antibodies detects a unique band
892 at 25kDa in RH Δ KU80 parasite lysate. **B-** Analysis of Rab11A localization in fixed
893 RH Δ KU80 parasites using antibodies recognizing Rab11A and IMC3 as indicated.
894 Bars: 1 μ m. **C-**Sequences of images extracted from movies SM1 and SM2 (left
895 images, white frames) showing the dynamic bi-directional movement of Rab11A-
896 positive vesicles in the cytosol (upper sequence) and along the parasite cortex (lower
897 sequence) of mcherryRab11A-WT and IMC3-YFP expressing parasites. Tracking of
898 vesicle trajectory is also shown. Images on the right show a zoom of the residual body
899 (RB) region indicated by a yellow frame in the corresponding vacuole. Bars: 2 μ m. **D-**
900 Sequences of images extracted from movies SM4 and SM5 (left images, white
901 frames) showing the dynamic movement of Rab11A-positive vesicles along the actin-
902 positive parasite cortex (upper sequence) and their interaction with dynamic F-actin
903 structures within the parasite cytosol (lower sequence) of mcherryRab11A-WT and
904 Cb-Emerald expressing parasites. Bars: 2 μ m. **E-** Images extracted from movie SM6,
905 where mcherryRab11A-WT and IMC3-YFP expressing parasites were treated with
906 cytochalasin D (CD) for 30 min before being recorded. Rab11A-positive vesicles
907 localized in *quasi* static clusters, as shown after tracking the trajectories. Bar: 2 μ m.

908

909

910 **Figure 2**

911 **A-** Image extracted from a time-lapse acquisition illustrating the release of SAG Δ GPI
912 protein (green) into the vacuolar space of mcherryRab11A-WT and SAG Δ GPI-GFP
913 expressing parasites, as well as the co-distribution in the parasite cytosol of
914 SAG Δ GPI-GFP positive DG and mcherryRab11A-WT positive vesicles (red). The
915 right insert shows a zoom of the region indicated by a white frame in the full vacuole.

916 Bar: 2 μ m. **B-** Fluorescence intensity profiles plotted over the distance of the GFP and
917 mcherry signals along the line indicated in A (insert). **C-** Percentage of co-distribution
918 between the total population of SAG Δ GPI-GFP-positive DGs and mcherryRab11A-
919 WT-positive vesicles of a given vacuole averaged over 5 consecutive time points
920 (n=10 vacuoles). Data show mean \pm sd. (**p<0,001). **D-** Sequences of images
921 extracted from movie SM7 (region indicated by a white fame in the full vacuole)
922 illustrating the joint motion of a Rab11A-positive vesicle (red) and a SAG Δ GPI-
923 positive DG (green) along the parasite cortex, as illustrated by their tracking. Time is
924 indicated in seconds. **E-** Automated tracking of all DG trajectories within the vacuole
925 (SM8). **F-** Three trajectories (1, 2, 3) (Movie SM9) in the region indicated by a white
926 frame in **E-** were analyzed by plotting the Mean Square Displacement (MSD) over Δ T
927 (s) using the Imaris software. Trajectory N $^{\circ}$ 2 (black line) corresponding to the track
928 shown in **-D** (SM7) fitted a mathematical model of “directed” motion (green line)
929 defined by the equation $MSD=4Dt+v^2t^2$ while trajectories 1 and 3 displays a
930 “confined” motions.

931

932 **Figure 3**

933 **A-** Western blot analysis with anti-Rab11A antibodies detects Rab11A-WT and
934 Rab11A-DN proteins in similar amounts after 4 h of Shield-1 induction (+S) of
935 intracellular tachyzoites. Eno2 is used as a loading control. **B-** Immunofluorescence
936 assay (IFA) showing the dense granule proteins GRA1 and GRA3 (green) retained in
937 intra-cytosolic vesicles following 2 h (upper panel) and 4 h (lower panel) of Shield-1
938 induction of Rab11A-DN parasites, while being efficiently released into the vacuolar
939 space and at the vacuole membrane in similarly induced Rab11A-WT parasites. The
940 parasite cortex is delineated by the glideosome protein GAP45 (red). Bars: 1 μ m. **C-**
941 Percentage of vacuoles positive for GRA1 and GRA3 secretion in Rab11A-WT and
942 Rab11A-DN parasites induced (+S) or not (-S) with Shield-1. Data show mean \pm
943 SEM of three independent experiments. **D-** Image extracted from movie SM10
944 illustrating DG movements in mcherryRab11A-DN / SAG Δ GPI-GFP expressing
945 parasites. DGs accumulate in the parasite cytosol and remain stationary along the
946 segregating membrane of daughter cells (arrows). Bar: 2 μ m. **E-** Images extracted
947 from movie SM10 illustrating the trajectories of 4 DGs analyzed in **F-**. **F-** Tracking of
948 DGs in Rab11A-DN expressing parasites indicates mostly confined (as exemplified

949 for DG trajectories 2, 3) and diffusive (trajectories 1, 4) motions. **G-** Mean diffusion
950 coefficient (D) calculated from 10 cortical trajectories manually tracked in Shield-1
951 induced Rab11A-WT and Rab11A-DN parasites. Data show mean \pm sd. (**p<0,01).
952 **H-** IFA showing the glucose transporter GT1 and Romboïd protein ROM4 (green)
953 retained in intra-cytosolic vesicles in Shield-1 induced Rab11A-DN parasites, while
954 being efficiently delivered at the plasma membrane in induced Rab11A-WT parasites.
955 The parasite cortex is delineated by GAP45 (red). Bars: 2 μ m.

956

957 **Figure 4**

958 Electron micrographs of infected host cells harboring Shield-1 induced Rab11A-WT
959 replicating parasites (**A**), in which dense granules (A1) and the IVN (A2) are
960 visualized. Shield-1 induced Rab11A-DN parasites (**B**) accumulate dense granules
961 (B1), notably at their basal pole and the IVN is not detected in the drastically reduced
962 vacuolar space. Rab11A-DN expressing parasites also display a previously described
963 defect in membrane segregation between daughter cells (**C**). A zoom of the regions 1
964 and 2 is shown in C1 and C2. Bars: 500nm.

965

966 **Figure 5**

967 **A-** Quantification of the percentage of Shield-1 induced extracellular Rab11A-DN
968 parasites adhering to host cells normalized to control Rab11A-WT parasites. Data
969 show mean \pm SEM of three independent experiments. (**p<0,01). **B-** Quantification
970 of the percentage of Shield-1 induced extracellular Rab11A-DN parasites, normalized
971 to control Rab11A-WT parasites, displaying a SAG1-positive trail deposit (green) as
972 illustrated in the images. Data show mean \pm SEM of three independent experiments.
973 (**p<0,001). **C-** Scanning Electron Micrographs (SEM) of Shield-1 induced
974 extracellular Rab11A-WT and Rab11A-DN parasites, which were allowed to move
975 for 15 min on BSA-coated coverslips before fixation. Arrows indicate the apical pole
976 of the parasite. Bars: 2 μ m. The histograms indicated the mean Circularity (upper
977 graph) and Aspect Ratio (major axis / minor axis) (lower graph) of Shield-1 induced
978 extracellular Rab11A-WT and Rab11A-DN parasites imaged by SEM (n=70 parasites
979 for each condition; ***p<0,001). **D-** Western blot analysis of excreted-secreted
980 antigen assays (ESA) performed with Shield-1 induced (+S) or not (-S) extracellular
981 Rab11A-WT and Rab11A-DN expressing parasites revealed a defect in MIC2 and

982 GRA1 protein secretion. Eno2 was used as a loading control. **E-** Quantification of
983 secreted MIC2 proteins (ESA fraction) and intracellular GRA1 proteins (pellet
984 fraction) from 3 independent ESA (as shown in **D-**) expressed in fold-change
985 compared to non-induced Rab11A-WT parasites (lanes 1 in **D-**) (* $p < 0,05$, ** $p < 0,01$).
986 **F-** Quantification of the percentage of Shield-1 induced extracellular Rab11A-DN
987 expressing parasites, which have invaded host cells normalized to control Rab11A-
988 WT expressing parasites. Data show mean \pm SEM of three independent experiments.
989 (* $p < 0,05$). Fluorescence images show Shield-1 induced mcherryRab11A-DN (red)
990 invading host cells, as illustrated by the presence of a circular junction positive for
991 RON4 (green). Bars: 1 μ m.

992

993 **Figure 6**

994 **A-** Sequences of images extracted from movie SM13 showing the polarized
995 recruitment of mcherryRab11A-positive vesicles (white arrows) towards two main
996 foci localized at the tip of adhering parasites (red arrows). Time is indicated in
997 seconds. Bar: 2 μ m. **B-** Sequences of images extracted from movie SM14 showing a
998 similar polarized localization of mcherryRab11A-positive vesicles (white arrows)
999 during host cell invasion. Time is indicated in seconds. Bar: 2 μ m. **C-** Fluorescence
1000 images of RH Δ KU80 parasites fixed at three different steps of the host cell invasion
1001 process, as illustrated in the right scheme. The circular junction is labeled with RON4
1002 (green) and the membrane protein SAG1 was used to label the extracellular portion of
1003 the invading parasite (red). Bar: 2 μ m.

1004

1005 **Figure 7**

1006 **A-** Immunofluorescence images showing the co-localization of the mcherryRab11A-
1007 positive signal (red) and GRA1-positive DG at two apical foci localized, where the
1008 Inner Membrane Complex (labeled with anti-GAP45 antibodies, white) interrupts, in
1009 motile extracellular induced Rab11A-WT (upper row). This apically polarized
1010 secretion is no longer detected in induced Rab11A-DN expressing parasites (lower
1011 panel). Bars: 2 μ m. **B-** A similar apical and focalized co-localization between Rab11A
1012 and SAGAGPI-GFP-positive DGs is observed during host cell invasion (illustrated by
1013 the detection of the RON4-positive circular junction). DG apical secretion is no
1014 longer observed in invading Rab11A-DN. Bars: 2 μ m.

1015

1016 **Supplementary Figure 1**

1017 **A-**Immunofluorescence assay showing the dense granule proteins GRA2 and GRA5
1018 (green) retained in intra-cytosolic vesicles in Shield-1-induced (+S) Rab11A-DN
1019 expressing parasites, while being efficiently released into the vacuolar space and at
1020 the vacuole membrane in induced Rab11A-WT expressing parasites. The parasite
1021 cortex is delineated by GAP45 (red). Bars: 2 μ m. **B-** Fluorescence images showing the
1022 dense granule protein GRA16 (green) retained in intra-cytosolic vesicles in Shield-1-
1023 induced Rab11A-DN expressing parasites, while being secreted and translocated into
1024 the host cell nuclei (small arrows) in induced Rab11A-WT expressing parasites. Bars:
1025 5 μ m. **C-** Immunofluorescence assay showing the localization of the non-secreted
1026 proteins GRA3 (red) and ROM4 (green) in distinct vesicles in Shield-1 (+ S) induced
1027 Rab11A-DN expressing parasites. In Rab11A-WT expressing parasites, both proteins
1028 are efficiently released at the vacuolar membrane and at the parasite plasma
1029 membrane. Bars: 2 μ m.

1030

1031 **Supplementary Figure 2**

1032 **A-**Immunofluorescence assay showing the correct localization of SAG1, GAP45 and
1033 MLC1 in Shield-1-induced extracellular adherent Rab11A-DN expressing parasites.
1034 Bars: 2 μ m.

1035

1036 **Supplementary Figure 3**

1037 Immunofluorescence assay showing the apical localization of MIC2-positive
1038 micronemes (A) and the plasma membrane protein ROM4 (B) in Shield-1 induced
1039 Rab11A-WT and Rab11A-DN parasites. Bars: 2 μ m.

1040

1041 **Supplementary Movie SM1 and SM2**

1042 mcherryRab11A-positive vesicle (red) dynamics (left panel) in intracellular *T. gondii*
1043 parasites expressing IMC3-YFP (green). Imaging speed: 2 fps.

1044

1045 **Supplementary Movie SM3**

1046 Movie showing mcherryRab11A-positive vesicles (left panel, arrows) moving along
1047 the developing daughter buds labeled with IMC3-YFP (right panel) during the process
1048 of cytokinesis. Imaging speed: 2 fps.

1049

1050 **Supplementary Movie SM4**

1051 mcherryRab11A-positive vesicle (red) dynamics in intracellular *T. gondii* parasites
1052 expressing Cb-Emerald GFP (green) showing a mcherryRab11A-positive vesicles
1053 moving along cortical F-actin. Imaging speed: 2 fps.

1054

1055 **Supplementary Movie SM5**

1056 Rab11A-positive vesicles (red) in close contact with dynamic cytosolic actin
1057 filaments in intracellular *T. gondii* parasites expressing Cb-Emerald GFP (green).
1058 Imaging speed: 2 fps.

1059

1060 **Supplementary Movie SM6**

1061 mcherryRab11A-positive vesicle (red) dynamics in intracellular *T. gondii* parasites
1062 treated with cytochalasin D for 30 min before imaging. Imaging speed: 2 fps.

1063

1064 **Supplementary Movies SM7 and SM7b**

1065 Movies showing the joint transport of a DG (green) docked on a Rab11A-positive
1066 vesicle (red) along the cortex of a SAG1 Δ GPI-GFP and mcherryRab11A-WT
1067 expressing parasite. SM8b: tracking of the vesicles.

1068

1069 **Supplementary Movie SM8**

1070 Automatic tracking of DG motion in SAG1 Δ GPI-GFP expressing parasites.

1071

1072 **Supplementary Movie SM9**

1073 Movie showing 3 DG tracks extracted from a region of interest of SM9 and analyzed
1074 for their mode of motion. Trajectory 2 (also shown in SM8) displays a directed
1075 motion, while trajectories 1 and 3 display confined diffusive motions.

1076

1077 **Supplementary Movie SM10**

1078 Dense granule (green) dynamics in intracellular *T. gondii* parasites expressing SAG1
1079 Δ GPI-GFP and mcherryRab11A-DN. The trajectories of 4 DG were tracked.

1080

1081 **Supplementary Movie SM11**

1082 Dense granule (green) dynamics in intracellular *T. gondii* parasites expressing SAG1
1083 Δ GPI-GFP and mcherryRab11A-DN 4h after Shield-1 removing in 0,5 μ M pre-
1084 induced Rab11ADN parasites. Imaging speed: 4 fps

1085

1086 **Supplementary Movie SM12**

1087 Dense granule (green) dynamics in intracellular *T. gondii* parasites expressing SAG1
1088 Δ GPI-GFP and mcherryRab11A-DN 4h after Shield-1 removing in 1 μ M pre-induced
1089 Rab11ADN parasites. Imaging speed: 2 fps.

1090

1091 **Supplementary Movie SM13**

1092 mcherryRab11A-positive vesicle (red) dynamics in Shield-1 induced extracellular
1093 motile *T. gondii* parasite. Imaging speed: 2 fps.

1094

1095 **Supplementary Movie SM14**

1096 mcherryRab11A-positive vesicle (left panel) dynamics in Shield-1 induced
1097 extracellular *T. gondii* parasite invading a host cell (right panel). Imaging speed: 2
1098 fps.

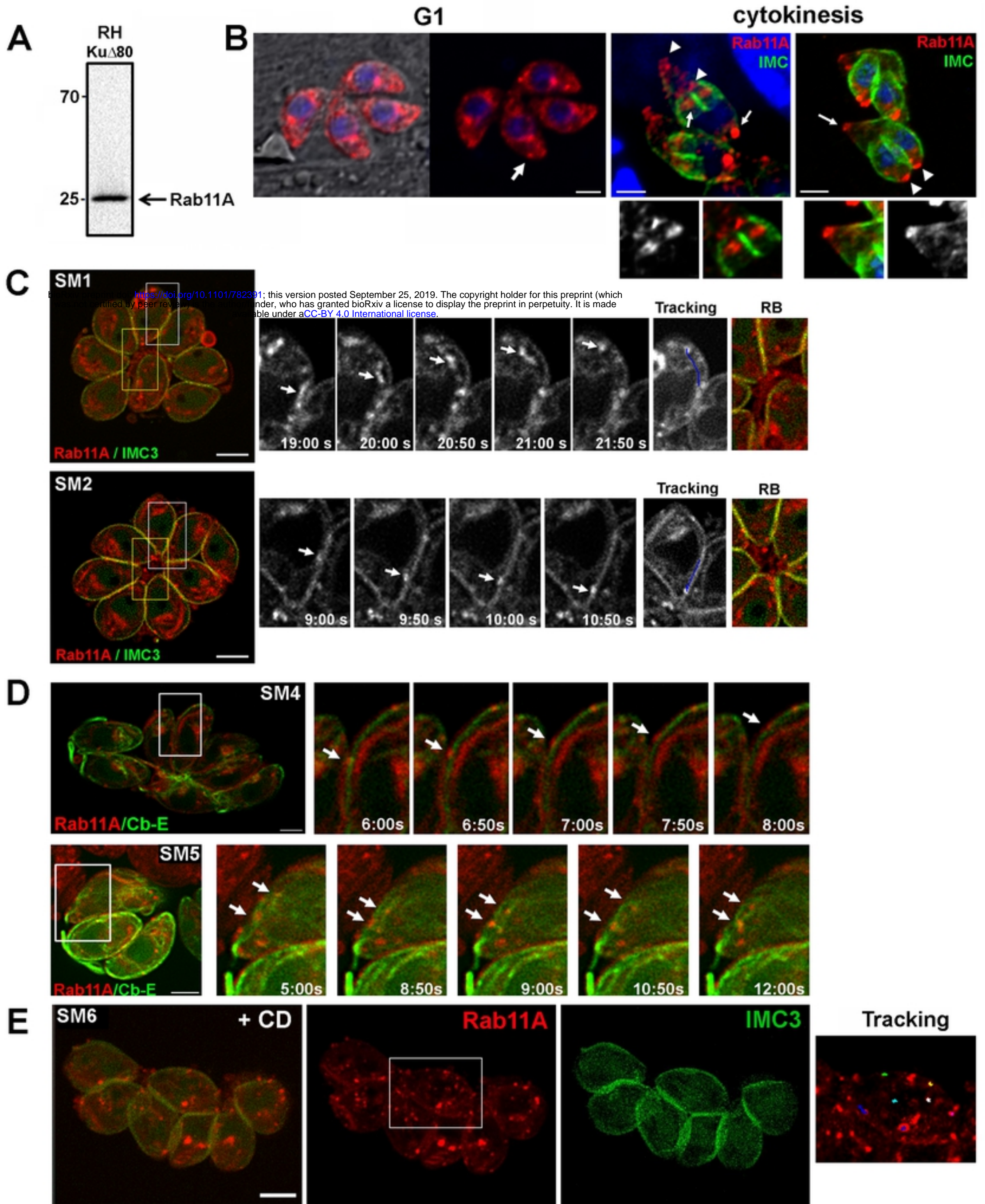


Figure 1

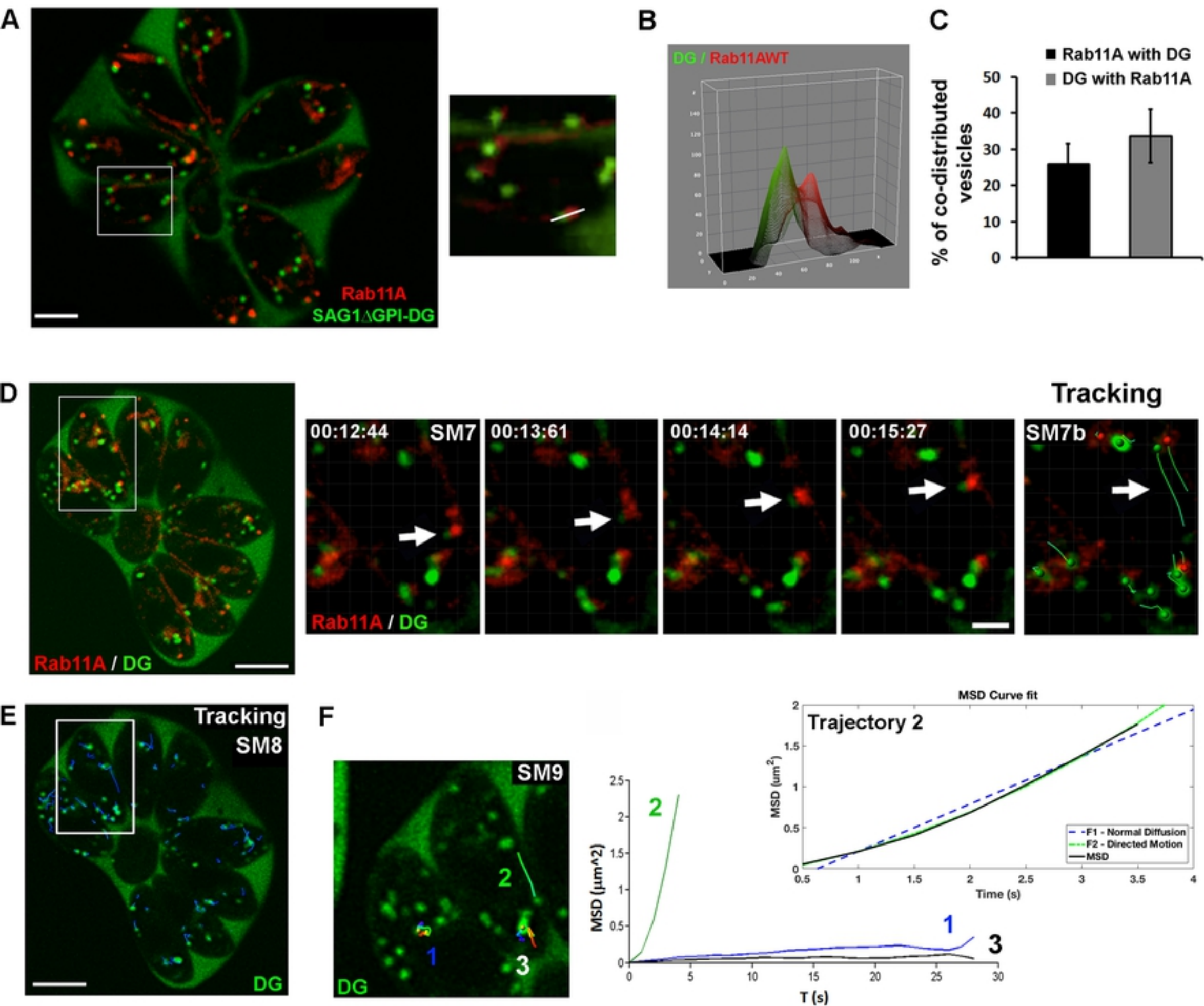
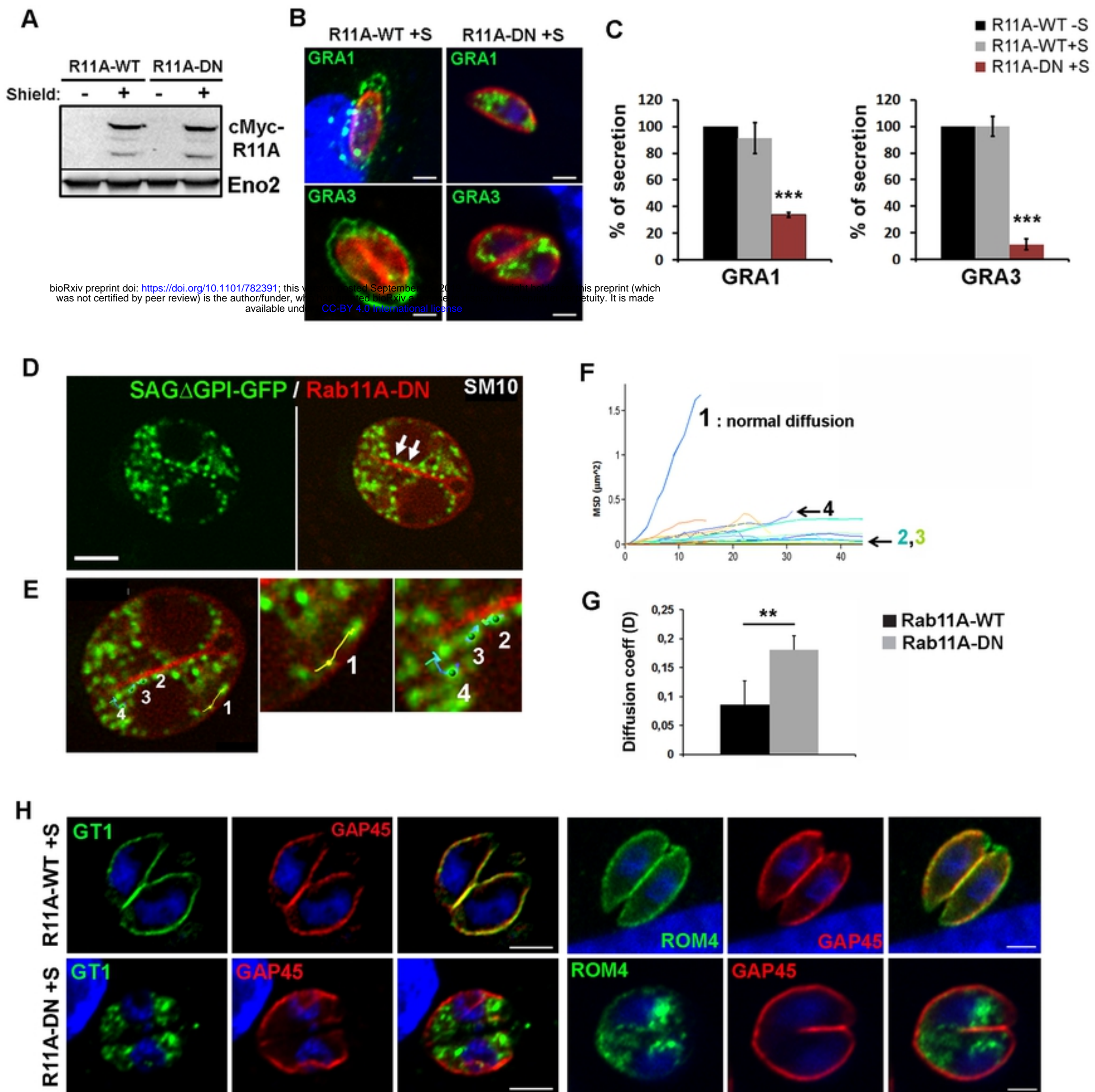


Figure 2



bioRxiv preprint doi: <https://doi.org/10.1101/782391>; this version posted September 20, 2020. The copyright holder for this preprint (which was not certified by peer review) is the author/funder, who has granted bioRxiv a license to display the preprint in perpetuity. It is made available under aCC-BY 4.0 International license.

Figure 3

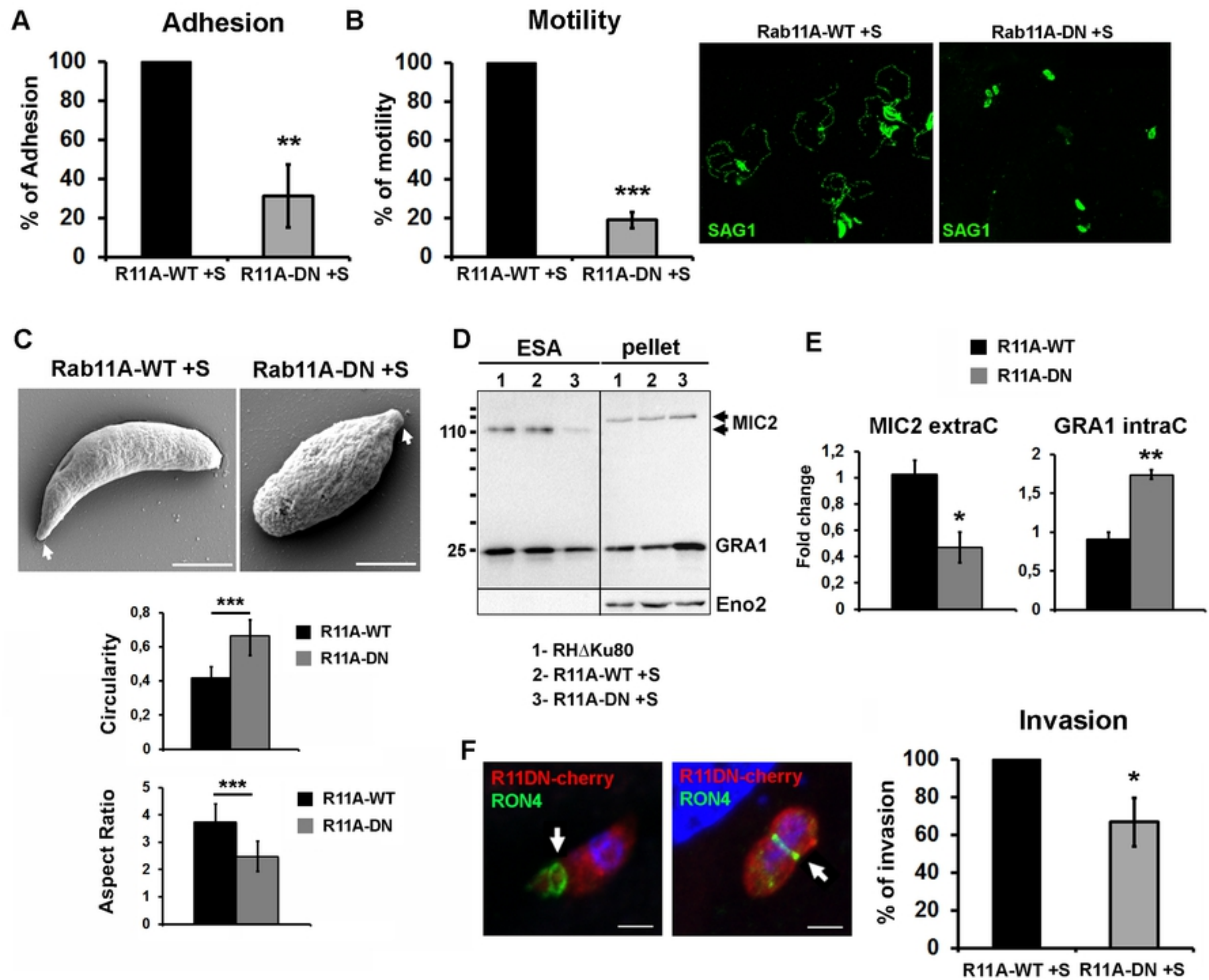


Figure 5

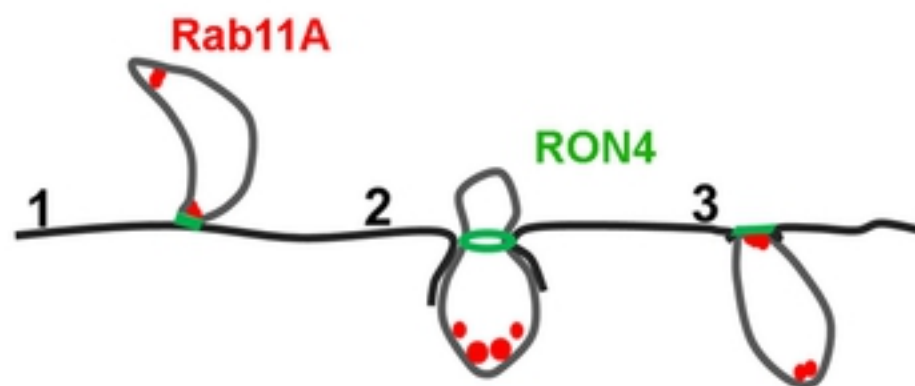
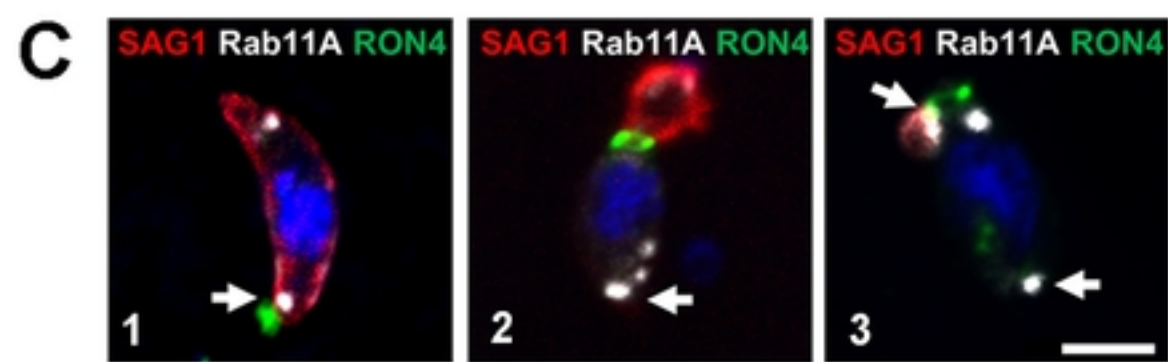
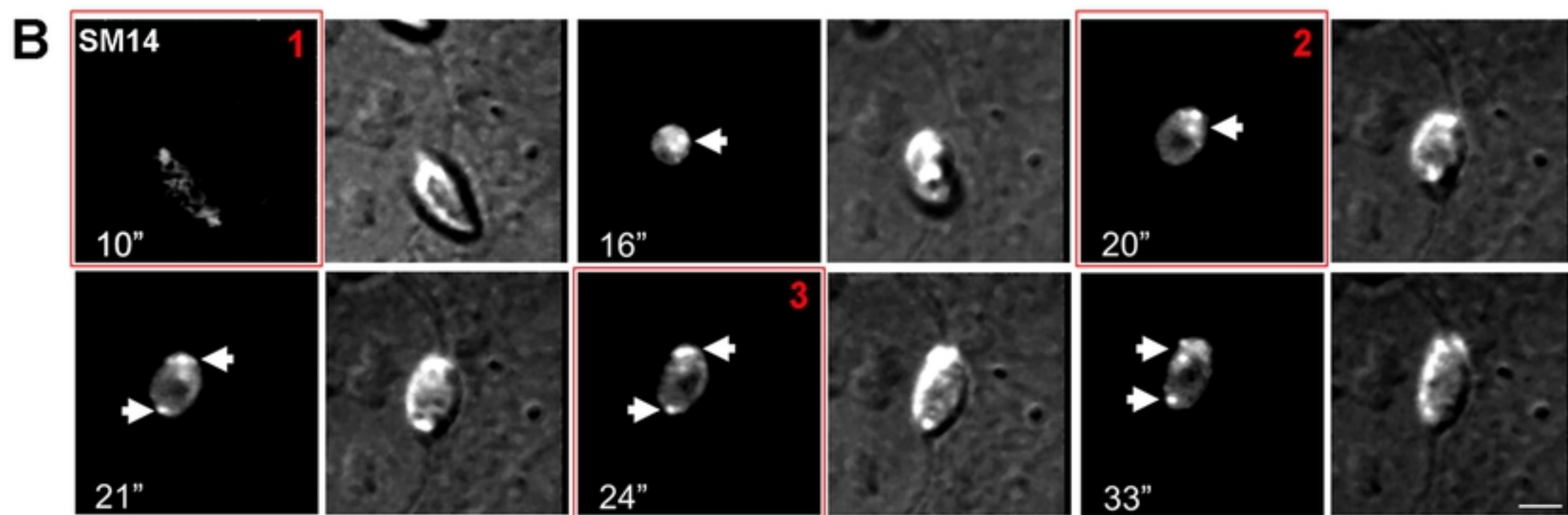
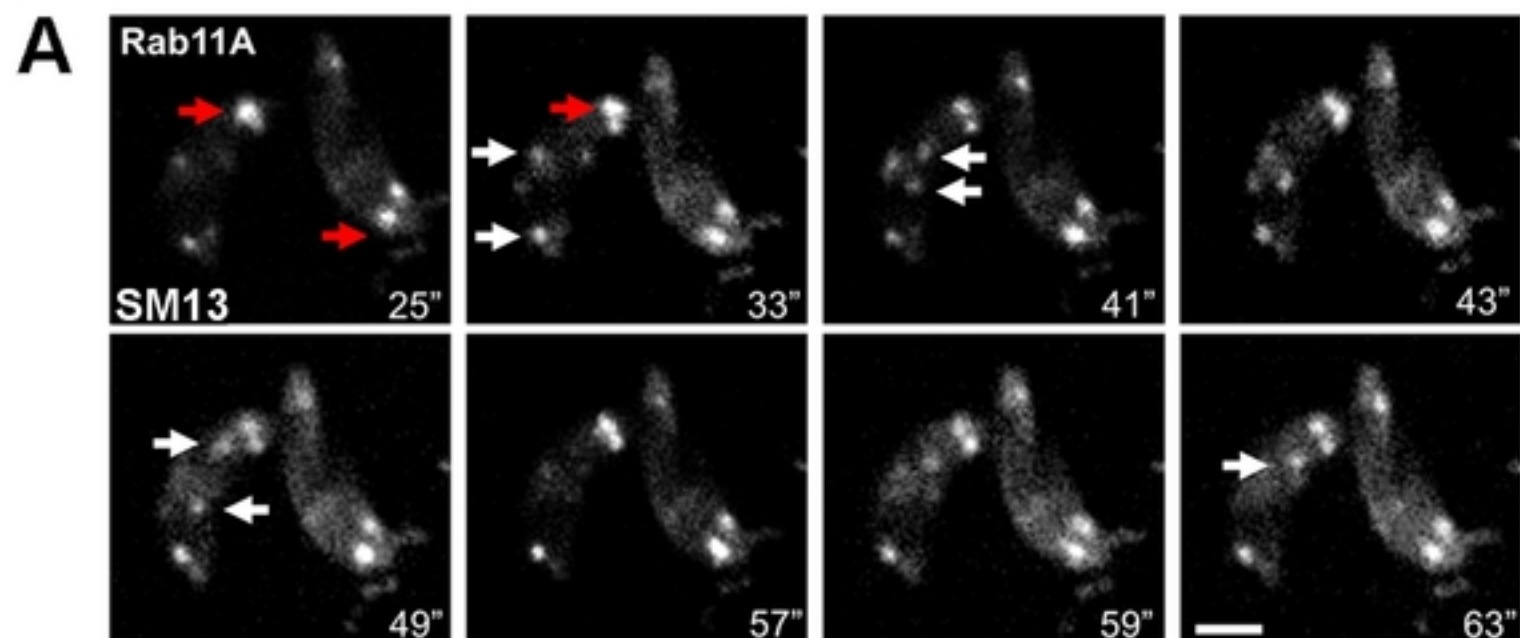


Figure 6

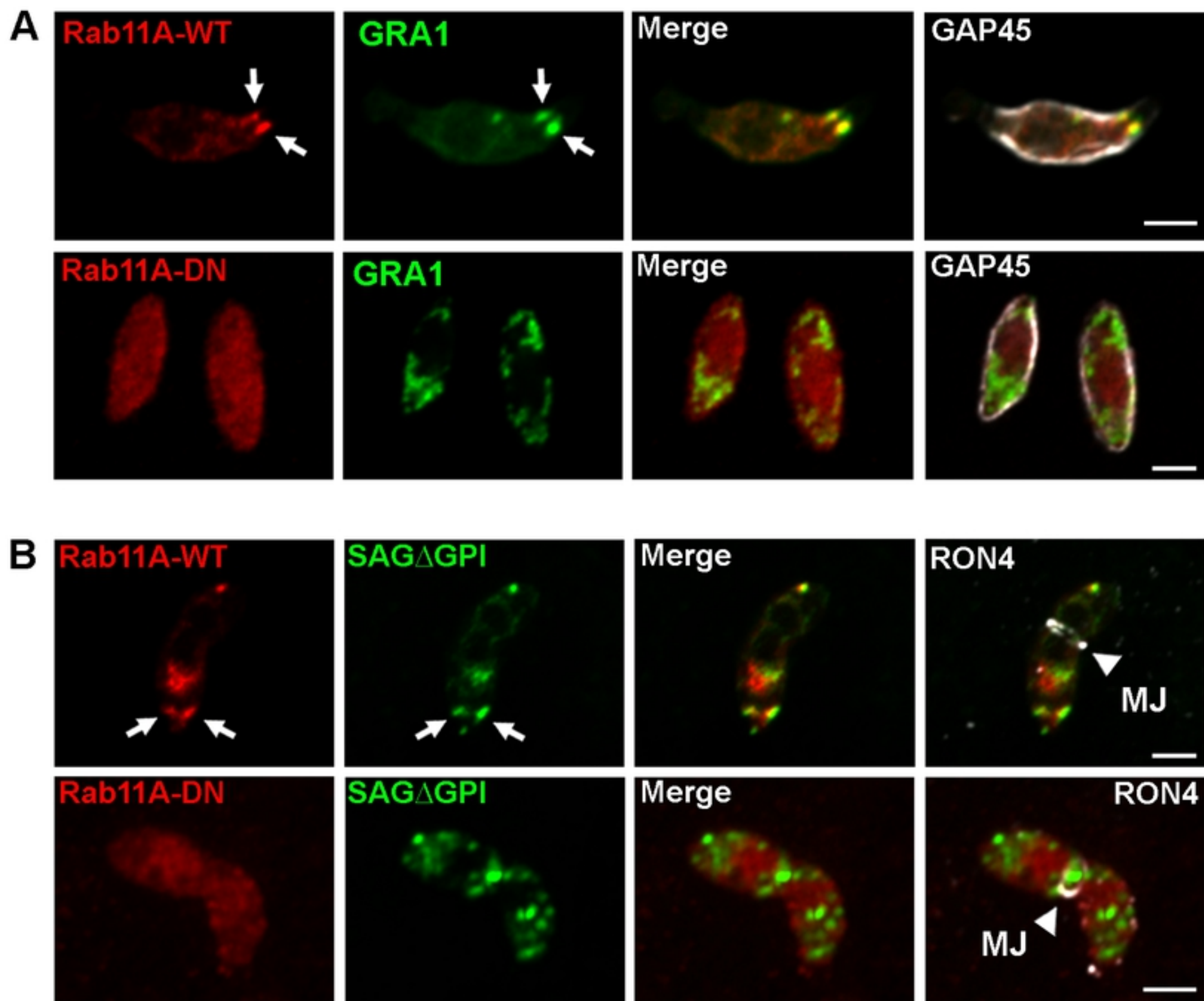


Figure 7

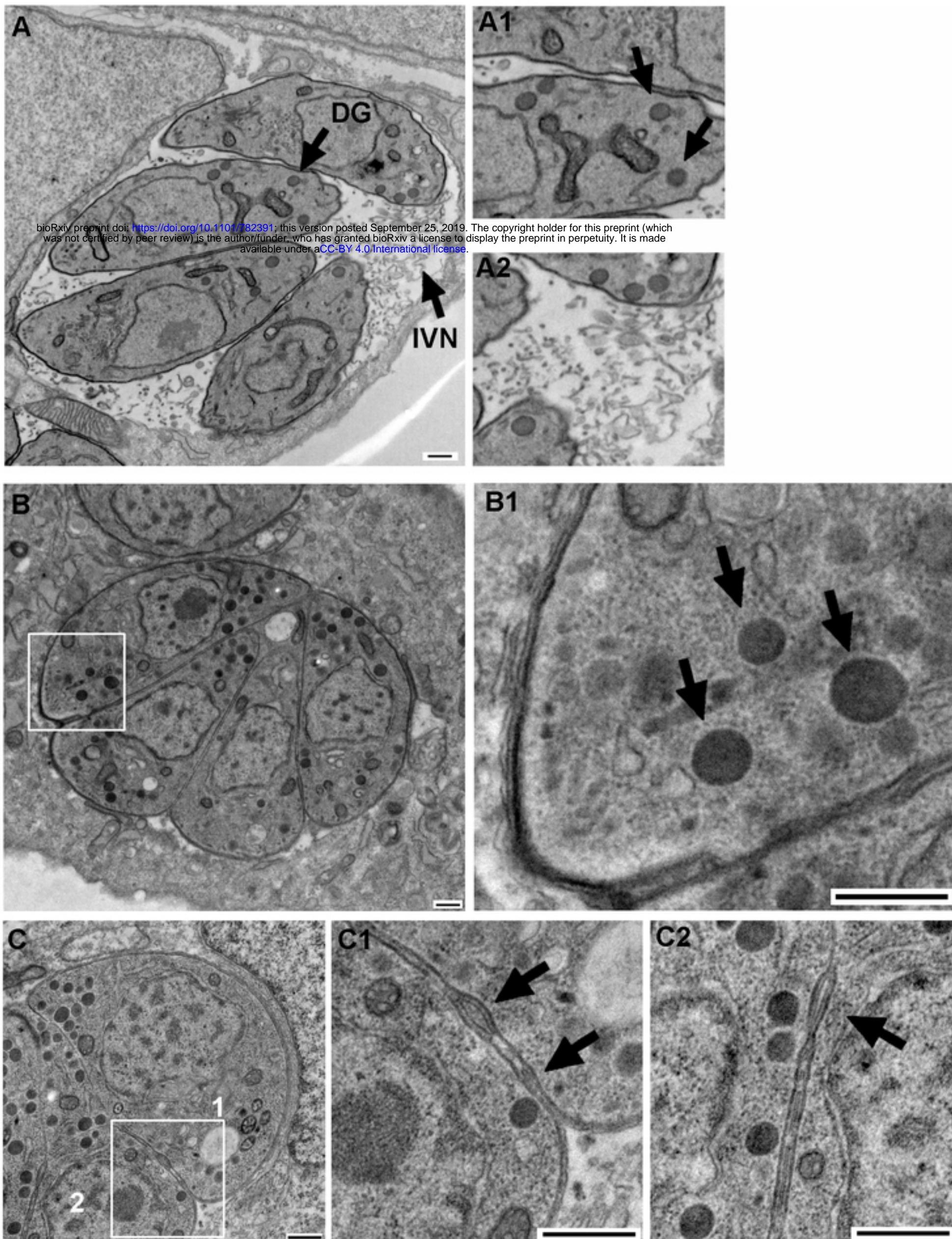


Figure 4